



# Ballast Settlement Accumulation in Zones with Unsupported Sleepers

Olga Nabochenko<sup>1</sup> · Mykola Sysyn<sup>1</sup>  · Szabolcs Fischer<sup>2</sup>

Accepted: 22 March 2024  
© The Author(s) 2024

## Abstract

The high influence of impact and vibration on the behavior of crushed stone and ballast materials has been known for a long time. The zones with unsupported sleepers, which are always present in transition zones, crossings, welds, etc., are typically characterized by impact interaction, ballast full unloading, and additional preloading. However, no studies on ballast layer settlements consider impact vibration loading. Moreover, the influence of the cyclic loading on the ballast settlement intensity is considered ambiguously, with both decelerating and accelerating trends. The comprehensive literature review presents the influence of factors on settlement intensity. The present study aims to estimate the long-term processes of sleeper settlement accumulation depending on the loading factors: impact, cyclic loading, and preloading. The typical for a void zone ballast loading pattern was determined for various void sizes and the position along the track by using a model of vehicle-track interaction that was validated by experimental measurements. The loading patterns were parametrized with four parameters: maxima of the cyclic loading, impact loading, sleeper acceleration, and minimal preloading. A specially prepared DEM simulation model was used to estimate the ballast settlement intensity after initial settlement stabilization for more than 100 loading patterns of the void zone cases. The settlement simulation results clearly show that even a low-impact loading pattern causes many times increased settlement intensity than ordinary cyclic loading. Moreover, the initial preloading in the neighbor-to-void zones can cause even a decrease in the settlement intensity compared to the full ordinary or partial unloading. A statistical analysis using a machine learning approach and an analytic one was used to create the model for the intensity prediction regarding the loading patterns. The analytic approach demonstrates somewhat lower prediction quality, but it allows to receive plausible and simple analytic equations of the settlement intensity. The results show that the maximal cyclic loading has a nonlinear influence on the settlement intensity that corresponds to the 3–4 power function, and the impact loading is expressed by the linear to parabolic function. The ballast's minimal preloading contributes to the reduction of the settlement intensity, especially for high cyclic loadings that are typical for neighbor-to-void zones. The results of the present study could be used for the

---

Extended author information available on the last page of the article

complementing of the present phenomenological equations with the new factors and further application in the algorithms of the settlements accumulation prediction.

**Keywords** Ballast layer · Unsupported sleepers · Void zones · Impact and vibration · Ballast full unloading · DEM simulation · Ballast loading patterns · Settlement intensity

## 1 Introduction

Sleeper voids or unsupported sleepers are one of the most frequent failure modes that cause quick deterioration of track geometry. Sleeper voids are usually initiated by inhomogeneities along the track that cause different ballast loading and differential settlements. The transition zones to bridges, culverts, underground communications, rail welds, and common crossings are always subjected to the appearance of sleeper voids and track irregularities (Kangle Chen 2022; Wang and Markine 2018; Oliveira Barbosa et al. 2022; Nasrollahi et al. 2023; Varandas et al. 2014; Chen and McDowell 2016; Kurhan et al. 2020). However, the prediction of track geometry and void development in the zones is complicated due to numerous acting factors, which results from many studies with quite different results.

Many last studies on rail-track dynamic interaction present detailed 3D FEM models and analysis of the dynamic behavior of the ballast layer (Khan and Dasaka 2023; Sayeed and Shahin 2023; Alzabeebee 2023; Moghadam and Ashtari 2020; Hadi and Alzabeebee 2023). However, the specific dynamic interaction due to void zones is usually not accounted for in the linear models or not explicitly analyzed in the nonlinear ones. The ballast vibrations were considered as only the result of wheel-rail interaction or ballast superstructure with subgrade under moving loadings. The vibrations were induced only by moving quasistatic loadings and not by geometric or void irregularities' ballast impact.

The short-term dynamic interaction in void zones was presented by numerous studies. The theoretical study (Lundqvist and Dahlberg 2005) presents a FEM simulation of the ballast-sleeper impact because of unsupported sleepers. Lundqvist and Dahlberg (Lundqvist and Dahlberg 2005) simulated several hanging sleepers with a void depth of up to 1 mm. The results show a growth of up to 70% in the sleeper-ballast force at the neighboring sleepers for a single-hanging sleeper with a 1-mm void.

An experimental investigation (Zhu et al. 2011) presents a 1:5 scale laboratory model and a numerical simulation model that was used to study the dynamic behavior of unsupported sleepers. Both experimental and simulation results demonstrate the growth in the dynamic interaction due to the unsupported sleepers.

In studies (Sysyn et al. 2020, 2021a), the dynamic behavior of railway tracks with sleeper voids in the ballast pulverization zone is presented. The evaluation of experimental data has shown a dynamic impact in voided zones, which appears due to the closure of the voids under the sleeper during the wheel passing in the voided zone.

The paper (Fang et al. 2023) develops a dynamic analysis framework combining the discrete element method (DEM) and the multi-body dynamic method (MBD). The model is used to simulate dynamic responses of the locomotive and ballasted tracks considering 0–5 unsupported sleepers. Simulations show that the acceleration of the wheelsets begins to increase when running to the position in front of the hanging area and increases to the maximum when running to the edge of this area. This effect was also experimentally measured and theoretically substantiated by the simulations in the studies (Sysyn et al. 2020, 2021a). The model does not explicitly present the impact on the hanging sleepers of the ballast bed due to the void closing. Nevertheless, the authors in the further paper (Fang et al. 2024) have also found the “dynamic impact” that has been in detail studied in Sysyn et al. 2021a some years before.

Ballast in void zones, different from the well-supported track, is subjected to different loading conditions (Fig. 1). The sleeper support along the track could be divided into the following zones (Sysyn et al. 2021a; Holtzendorff 2003; Popp 2003). The ballast under the hanging sleepers is on the one side fully unloaded and subjected to impact loadings in sleepers before the wheel during the void zone. On the other side, the neighbor zones carry the hanging part of the track, and they are subjected to overloading.

The effects of the ballast full unloading and impact loading on the sleeper’s settlement intensity were noted in various studies. Authors Baeßler and Rucker (Baeßler and Rucker 2002) have examined in the full-scale test the influence of cyclic loading, partial sleeper unloading, and the impact loading on the sleeper settlement behavior. The test showed that the application of impact loading without full unloading increases the sleeper settlement intensity up to 4.2 mm/10,000 cycles. In comparison, the intensity under the cyclic loading with amplitude 35 kN was 0.06 mm/10,000 cycles. Moreover, the following application of full unloading together with impact one has increased the settlement intensity to 14.5 mm/10,000 cycles. The intensive vertical settlements were accompanied by

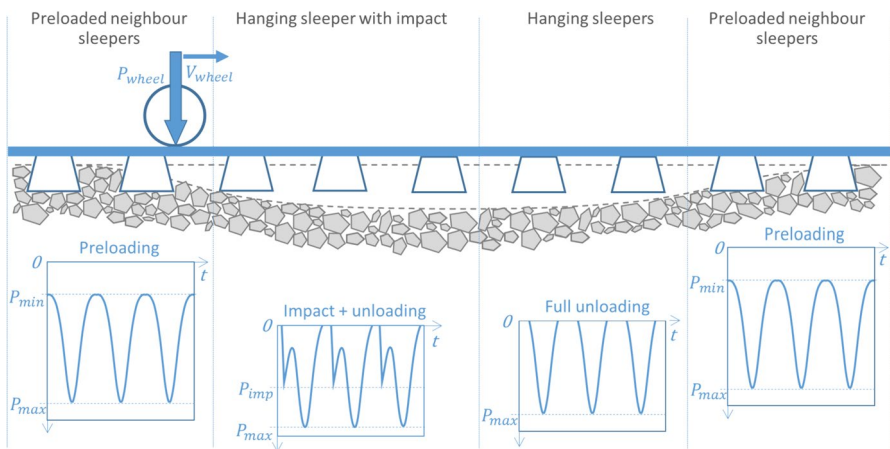


Fig. 1 Ballast loading in zones along the void

notable horizontal movement of the ballast material in the ballast shoulders, indicating the ballast flow. The decrease in ballast stiffness with increasing unloading was observed in the triaxial tests by Selig and Waters (Selig and Waters 1994). The authors showed that the degree of cyclic unloading influences the ballast confinement. The original tension is lost so that the stiffness of the ballast layer and, thus, the residual horizontal stress is reduced. However, the influence of the ballast unloading mode on the sleeper settlement intensity was not quantified.

### **1.1 The Influence of Impacts and Vibration on the Settlement Behavior of the Railway Ballast Layer**

The high influence of impacts and vibration on the settlement behavior of the ballast layer is known from many studies (Holtzendorff 2003; Popp 2003; Pahnke 2010). It was shown that the residual ballast settlements depend on the level of accelerations or excitation frequency. Some authors propose a limit value of the level of acceleration of 0.8 g for ballast bed on bridges. Other researchers perform studies with harmonic fundamental excitation of the ballast sample. In general, the result is a threshold value for destabilization and subsidence of approximately 1 g (Popp 2003). The destabilization involves a rapid change in the contacts between particles. From the performed experiments, it is concluded that the influence of the load frequency parameter is not decisive. With an increase in the frequency of acceleration in the ballast layer and other elements, the tracks can be redistributed, which will lead to a decrease in the acceleration in the ballast layer. More important is the simultaneous influence of such parameters as the load level, acceleration, and duration of the vibration load.

The problem of taking into account the effects of vibration loading consists of the difficulty of separating the different mechanisms that lead to increased settlement intensity. Thus, authors (Baeßler and Rücker 2002), separately from the basic track load, assume two types of vertical dynamic load on the ballast: the impact vibration load on the sleeper with backlash and the sleeper with good support.

Thus, the unloading mode of the ballast, vibration, and cyclic loading should be considered as independent factors of ballast resilience that cannot be replaced by taking into account only maximal cyclic loading.

### **1.2 Present Approaches for Prediction of Differential Settlements and Factors Taken into Account**

The prediction of long-track geometry deterioration and differential settlements is considered in many studies by using different phenomenological equations together with finite element method (FEM) and multibody simulation (MBS) models for ballast loading calculations.

The phenomenological models are based on empirical equations that are fitted to laboratory or in situ experimental data. The exponential and logarithmic forms are the most popular equations, but there were also linear and physical-based forms used the last time. There are two major stages of ballasted track settlement, as indicated

by many authors (Sato (Sato 1995), Dahlberg (Dahlberg 2001), and Grossoni (Grossoni et al. 2021)). The first stage is the initial settlements after tamping caused by ballast volume changes during the compaction process of the ballast layer. The stage of initial settlements could be partially shortened by machine compaction with dynamic stabilization. The settlement intensity in the second stage is approximately constant, and the stage is explained by the lateral movement of the ballast particles, deformation of the subgrade, particle attrition, breakage, etc.

However, the variance of the predicted settlements in the literature and even the variance of the measured settlements in the same experimental tests are high. Figure 2 shows the range of the predictions of the settlement accumulation by the present phenomenological models for the in situ measurements and full-scale tests (Grossoni and Andrade 2019; Lichtberger 2005). The high range of variance from about 1 to 16 mm for 500,000 of load cycles could be explained by different test conditions. Thereby, the highest variation, 1–13 mm, is observed during the initial stage until 100–200,000 cycles. The variance of the settlement intensity in stage 2 is more definite and amounts to 0.001–0.09 mm/10,000 cycles. Moreover, a significant variance of the settlements accumulation was observed among parallel experimental tests in Kangle Chen 2022; Demharter 1982).

Figure 2 (middle zone) demonstrates the range of measurement results from the six repetitions. The author (Demharter 1982) has concluded that the variance could not be eliminated even though all starting conditions were controlled carefully. It is notable from the experimental studies that despite the high variation of the initial settlements of 4.9–8.7 mm in stage 1, the settlement intensity in stage 2 has a comparatively low variance of 0.014–0.018 mm/10,000 cycles.

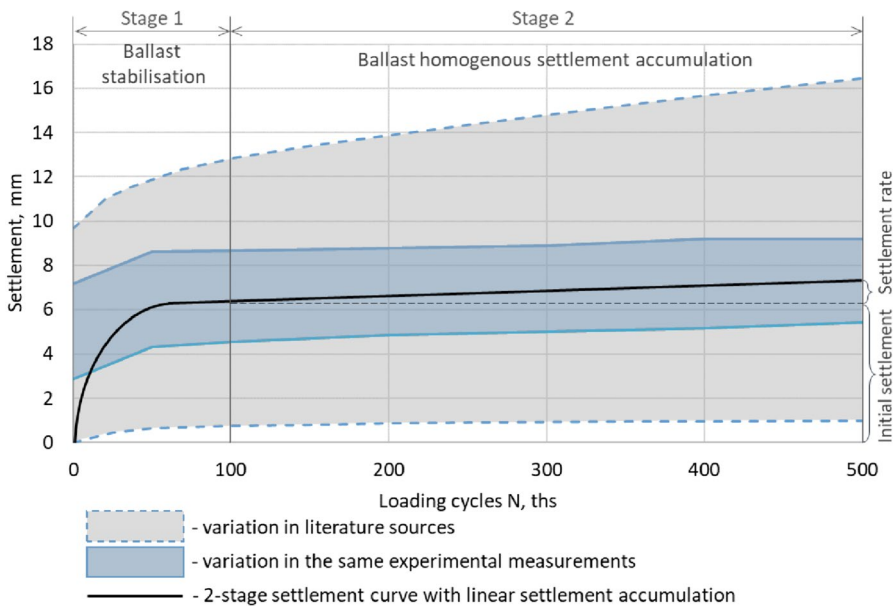


Fig. 2 Variation range of the predicted and measured settlement accumulations

The high variation of the settlements in stage 1 could be explained by the different initial compaction of the ballast and the uncertainty of the starting point of the measurement after the stabilization process.

Most authors suppose one phenomenological equation for both stages. However, the equations include mostly two parameters, of which one of them implicitly corresponds to the prediction of the quick deterioration in the initial stage. Nevertheless, the high variance of the measurement results makes it not possible to conclude about the best approximation. Independently on the complexity of the equations, both the exponential and logarithmic forms provide no advantage compared to the linear equations. Some authors (Wang and Markine 2018; Jeffs et al. 1987) prefer linear form that has the advantage of better interpretation. The ability to predict the settlements is determined not by the form of the phenomenological equation but by the factors taken into account. However, most phenomenological equations consider a very limited number of factors like loading cycles and maximal cyclic loading. The maximal loading is usually considered as the main factor of the settlements. Table 1 shows a summary of the phenomenological models and the main factors taken into account.

A systematization of the factor influence of the ballast settlements in void zones is presented in Holtendorff (2003). The proposed model of differential settlements and void development is based on a logarithmic phenomenological equation together with MBS and FEM models. The coefficients of the equation take into account the influence of different factors: equivalent vertical stress due to cyclic loading, dynamic factor due to impact and vibration, the degree of relief of the ballast due to full or partial sleeper unloading, the pollution factor, and initial compaction in the form of the passed loading cycles. However, the study considers the factors qualitatively, and the necessity of the experimental data for model calibration and verification is stated.

As proposed by ORE (ORE 1970) using the triaxial cyclic tests, a semi-logarithmic stress–strain equation suggests the quadratic relationship to the maxima of the cyclic load. Another logarithmic equation in the study (Shenton 1984) supposes a linear influence of the loading on the wheel loading on the settlement accumulation. An empirical coefficient suggests the subgrade properties and the sleeper form, and the tamping lift is considered directly in the equation. The linear influence of the pressure is presented in Thom and Oakley (2006) by a full-scale ballast box test. Additionally, the influence of the subgrade stiffness is explicitly considered in the equation.

The phenomenological equation in Fröhling (1997), which was developed in the course of an extensive measurement in track, takes into account the measured average track stiffness at a particular sleeper and dynamic load amplification with the exponent 0.3.

Ballast compaction is taken into account in Stewart and Selig (1984); Indraratna and Nimbalkar (2013) by using empirical coefficients for loose and dense ballast in a logarithmic equation. Indraratna et al. (Indraratna et al. 2007) displayed the influence of the relation of the deviatoric stress to the compressive strength of ballast with the exponent 1.12 to 1.67, depending on the ballast material. Hettler (Hettler 1987), based on scaled laboratory tests, presented a similar exponent of the loading 1.6 in a logarithmic equation.

**Table 1** Summary of the phenomenological models and the factors taken into account

Settlement equa- tion type	Author	Initial settle- ments in stabi- lization phase (< 100,000 cycles) (mm)	Settlement rate in phase of lin- ear settlement accumulation (> 100,000 cycles) (mm/10,000 cycles)	Factors taken into account				
				Max. cyclic loading $p$ on the ballast/sleeper	Subgrade stiff- ness, ballast bed material, conditions	Vibration, impact	Unloading mode/minimal loading	Ballast initial compaction/set- tlements or main- tenance issues
Logarithmic	ORE (1970)	-	-	-	-	-	-	-
	Shenton (1984)	5.9–6.6	0.162	-	+/-	-	-	+/-
	Fröhling (1997)	13.3–16.5	0.034	-	+	-	-	-
	Thom and Oak- ley (2006)	1.9–6.6	0.068	-	+	-	-	-
	Indraratna and Nimbalkar (2013)	9.8–11.9	0.026	-	-	-	-	+/-
	Stewart and Selig (1984)	7.1–8.3	0.012	-	-	-	-	+/-
	Shahin (2009)	-	-	-	-	-	-	-
	Hettler (1987)	-	-	-	-	-	-	-
	Holtzendorff (2003)	-	-	-	+/-	+/-	+/-	+/-
	Sato (1995)	11.2–14.3	0.151	-	-	-	-	+/-
	Selig and Waters (1994)	6.2–11.7	0.087	-	-	-	-	+/-
	Indraratna et al. (2007)	10.0–12.8	0.042	-	-	-	-	-
	Cuellar and Estaire (2011)	0.9–1	0.002	-	-	-	-	-

**Table 1** (continued)

Settlement equa- tion type	Author	Initial settle- ments in stabi- lization phase ( $< 100,000$ cycles) (mm)	Settlement rate in phase of lin- ear settlement accumulation ( $> 100,000$ cycles) (mm/10,000 cycles)	Factors taken into account				
				Max. cyclic loading $p$ on the ballast/sleeper	Subgrade stiff- ness, ballast bed material, conditions	Vibration, impact	Unloading mode/minimal loading	Ballast initial compaction/set- tlements or main- tenance issues
Linear	Wang and Markine (2018)	–	0.008	$p^{5.276}$	–	–	–	–
	Jeffs et al. (1987)	12.5	0.015	–	–	–	–	–
	Kumar et al. (2021)	–	–	$\sim p^{1.6}$	–	–	–	–



Table 1 (continued)

Settlement equa- tion type	Author	Initial settle- ments in stabi- lization phase (< 100,000 cycles) (mm)	Settlement rate in phase of lin- ear settlement accumulation (> 100,000 cycles) (mm/10,000 cycles)	Factors taken into account				
				Max. cyclic loading $p$ on the ballast/sleeper	Subgrade stiff- ness, ballast bed material, conditions	Vibration, impact	Unloading mode/minimal loading	Ballast initial compaction/set- tlements or main- tenance issues
Physical based, iterative	Oliveira Barbosa et al. (2022)	2.4–4.9	0	+	-	-	-	-
	Nasrollahi et al. (2023)	1.5	0.016	$\sim p$	-	-	-	-
	Sysyn et al. (2018)			$\sim p^3$	+	-	-	+
	Nguyen et al. (2016)	3	0.12	+/-	-	-	-	+/-
	Varandas et al. (2014)	7.1–8.3	0.012	$\sim p^{1.6}$	-	-	-	+
	Guerin et al. (1999)	1.9–3.2	0.010	$\sim p^{2.51}$	+/-	-	-	-
	Ognibene et al. (2022)	5–6	0.026	$\sim p$	-	-	-	-
	Punetha and Nimbalkar (2023)	18–29	0.066	+	+	-	-	-
	Grossoni et al. (2021)	-	-	$\sim p$	+	-	-	-

+/- = qualitatively considered or by empiric coefficients

The initial compaction is not taken into account in the equations. Therefore, the variation of the predicted settlements in the initial phase ( $< 100,000$  t) by different studies is very high.

The exponential settlement equation in Sato (1995) takes explicitly into account the factors of loading, velocity, subgrade, ballast depth, etc. Thereby, the linear settlement intensity is considered after the ballast stabilization phase. A similar approach with a linear equation in the second stage after 200,000 loading cycles is proposed in Jeffs et al. (1987).

The authors in Kumar et al. (2021) have used a linear model with the settlement intensity rate based on the logarithmic equation (Hettler 1987), the same exponent of the ballast loading. The equation was used together with a 2D vehicle-track interaction dynamic model to predict track geometry deterioration.

The authors in Wang and Markine (2018) assume the linear process of the settlement accumulation for modeling the long-term behavior of transition zones. The authors fully ignore the initial nonlinear settlement stage. Thereby, they used a high exponent of 5.276 of the ballast pressure in the linear phenomenological settlement equation. The exponent was estimated by fitting to the experimental data of other studies. Such a high exponent of the pressure allows reflection of the experimentally measured dips on two sides of transition zones at the late stage of the degradation. However, the overestimated influence of the ballast pressure could cause the locally over-dimensioned growth of the settlements under the separate sleepers without the growth in the neighboring ones.

The physical-based methods, different from the empirical phenomenological models, have a clear mechanical background. The study (Oliveira Barbosa et al. 2022) demonstrates a 2D lattice model able to describe the compaction behavior of railway ballast. The model is based on connection as a parallel assembly of a linear spring, a spring-slider couple, and a spring-gap couple and is able to reflect cyclic residual settlements. The model of the ballast box after calibration was integrated into the track model for the transition zone. The simulation results are compared to other studies and show a deviation that corresponds to the typical one in the studies (Fig. 2). The main problem of the 2D is that, despite the physical background, it is not able to reflect the intrinsic processes of ballast settlement due to the particle flow along across the track.

The study (Nasrollahi et al. 2023) presents an iterative approach for the prediction of long-term differential track settlement in a transition zone. The accumulation of ballast settlements depends on the difference between the maximal dynamic loading and the threshold loading with some exponent. There is no accumulation of permanent ballast/subgrade deformation if the maximum sleeper-ballast contact force generated by a passing wheel is below a certain threshold value. The value itself is dependent on the accumulated settlement with the negative exponential relation. Therefore, the settlements in the first 5–8 sleepers near the slab foundation have a quicker settlement rate than outside. Thus, the close-to-realistic dip shape is formed. The used exponent of ballast loading is 1. However, the used negative exponential relation assumes the full settlement stabilization. The direct influence of the vibration and other factors is not considered.

Nguyen et al. (Nguyen et al. 2016) elaborated a computational procedure for the prediction of ballasted track profile degradation. A hypoplastic model was integrated into a 2D track-train dynamic model. The model is formed by the combination of two constitutive laws: a hysteretic model and an accumulation model. It takes into account strain amplitude, void ratio, average mean pressure, average stress ratio, etc. The model demonstrates the declining character of the settlement accumulation. However, the authors did not explore the development of the void under the sleeper.

Varandas et al. (Varandas et al. 2014) presented the simulation of the void development along the transition zone and the comparison with experimental measurements. The ballast settlement equation takes into account the loading history that allows, in case of the loading increase, to reflect the realistic settlement accumulation with local stabilization periods. The settlement intensity of the ballast is proportional to the amplitude of the applied load with the exponent 1.6. The initial ballast settlements can be also taken into account in the loading history. Another iterative approach is proposed in Guerin et al. (1999) based on small-scale experiments with a sleeper and ballast box on an elastic base. The development of the settlement was split into two phases: phase 1 results from the compaction of the material, and the settlement development in phase 2 corresponds to the track in operation. The developed equation presents the settlement intensity as a function of the sleeper elastic deflection with the exponent 2.51. Thus, the equation takes into account implicitly both ballast loading and its stiffness.

A rheological approach for predicting the behavior of transition zones in a railway track is presented in Punetha and Nimbalkar (2023). The 3D FEM model was used together with plastic slider elements to reflect the residual settlements after reaching the satisfied yield criterion. The hardening rule and unloading phase are considered for ballast, sub-ballast, and subgrade. The simulation results present the declining to some limit settlement trend that depends on the axle loading and the smoothed over about 1.5-m settlements from the open track to the bridge in the transition zone. An increase in the axle loading causes an increase in the initial plastic settlements but a low impact on the settlement intensity. The void development was not shown in the study.

The application of a simplified rheological approach for the prediction of differential settlements is shown in the studies (Sysyn et al. 2018; Sysyn et al. 2019). The parallel connection of plastic and viscous elements describes the permanent deformation. The plastic element describes the initial settlements or the quick settlement while the loading increases over the threshold defined by the history of the ballast loadings. The plastic and viscous properties depend on the ballast loading with the polynomials of 2–3 exponent. However, the models do not take into account the void development and the resulting sleeper-ballast impact with the unloading mode.

Another paper that considers stress history using a linear Kelvin–Voigt unit in series with a plastic-hardening unit is presented in Ognibene et al. (2022). The ballast layer is modeled by combining a nonlinear visco-elastic element to simulate the resilient response with a plastic-hardening element for permanent settlement. Such an approach explicitly considers two intrinsic processes of permanent deformation: the initial densification and the long-term lateral spreading of the ballast. The model provides a realistic settlement process in case of a loading increase. However,

the model does not take into account the influence of vibration loading and ballast unloading mode.

The analysis of the present approaches of ballast settlement estimation shows a wide range of equations with quite different observed values of the settlement predictions. Indeed, even the same experimental studies show such high settlement variance that the different approaches can be described equally well. Most of the models explicitly consider the influence of one factor—the ballast loading. Thereby, some other factors like stiffness and maintenance issues are considered implicitly with the different coefficients in the equations. However, the influence of the ballast loading is not unambiguous, with the exponent variance from 0.3 to 5.12. Moreover, the direct settlement influence of the vibration, impact, and sleeper unloading, which appear in the void zones, was almost not considered in the settlement equations. The impact loadings are usually handled the same as cyclic loading. Therefore, there is no detailed understanding of the mechanisms of the deterioration of track geometry in zones with voids.

### 1.3 DEM Simulations of the Permanent Settlement Accumulation

DEM is increasingly used in the last time for simulating ballast settlements. Different from the empirical phenomenological equations that have low mechanical substantiation, the discrete element method allows consideration of the intrinsic mechanical processes.

Chen and McDowell (Chen and McDowell 2016) applied the discrete element method to investigate transition zones from a micromechanical perspective. A ballast box with three half-sleepers is regarded as a model of the transition zone. Two kinds of transition patterns, including a single-step change and a multi-step change for subgrade stiffness distribution, were tested. The influence of train direction, speed, and axle load on the transition zone was also investigated. The subgrade stiffness inhomogeneity was analyzed. The differential settlements were examined in 50 loading cycles, and high settlements imply that the ballast was fully uncompacted. However, the elastic influence of the rail was not defined; thus, the hanging sleepers were not taken into consideration. The ballast box had no free slopes; thus, the model could not take into account the sleeper settlements due to the ballast flow along the sleeper.

Another paper (Lobo-Guerrero and Vallejo 2006) presents 2D DEM simulations to study the effect of crushing on the behavior of a simulated track ballast material. The model displayed three sleepers under cyclic loading within 200 cycles. The ballast fragmentation was detected as the main factor of sleeper settlements, and the particle flow was not analyzed.

Fang et al. (Fang et al. 2023) introduced a model combining the DEM and MBD for the simulation of 0–5 sequentially unsupported sleepers within 15 ones in the already mentioned paper. However, the authors did not investigate the long-term processes of ballast settlement.

Tutumluer et al. (Tutumluer et al. 2013) used in the study DEM model for predicting the settlement behavior of full-scale test sections under repeated heavy

axle train loading. The settlement predictions were sensitive to aggregate shape, gradation, and initial compaction condition density of the constructed ballast layer. The number of simulation cycles was limited to 2000 loading cycles. It is indicated that by properly accounting for the initial compaction conditions, the ballast DEM simulations closely predicted the settlement performance with only 2000 car passes. The initial compaction in the DEM model corresponded to 580,000 loading cycles in the experimental measurements.

The researchers (Talebiahooie et al. 2021; Chen et al. 2015) have studied the settlement behavior of a half-sleeper in a square ballast box. The changes in ballast porosity and pressure were analyzed during 1000 loading cycles. However, the models had no free slopes that did not take into account the lateral spreading of the ballast along the sleeper.

Bian et al. (Bian et al. 2020) presented the principal stress rotation effect using DEM simulation of the 30-cm wide ballast box with five sleepers. The authors applied two different loading scenarios of the sleepers' loading: stationary cyclic and moving wheel loading. Numerical results indicated that moving wheel loading induced larger principal stress rotation than under stationed cyclic loading. Moreover, the permanent settlements of the sleepers during 500 loading cycles were more than four times higher for moving wheel loading. However, the quasi-2D model also was not able to take into account the lateral spreading of the ballast.

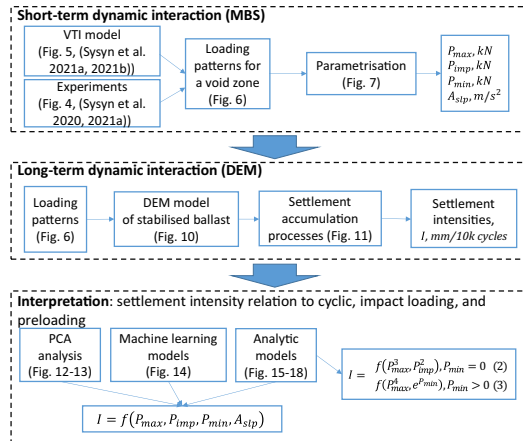
The study (Zhang et al. 2019) indicated the importance of load frequency in applying cyclic loads to investigate ballast deformation under high-speed train loads. Despite a relatively small-scale ballast box with a 30-cm part of sleeper in the DEM model, it clearly shows the increase of the settlement intensity for the loading frequency of more than 15 Hz. Thus, the factor of vibration is an independent one that directly influences ballast resilience and cannot be taken into account through the maximal loading amplitude. Moreover, the influence of vibration and loading can be reciprocally amplified.

The analysis of the present studies on long-term settlement accumulation using DEM shows that the models can take into account the main processes of ballast compaction, breakage, and flow and consider many factors of the loading, ballast material, geometrical size, etc. Therefore, the DEM models could be most appropriate for the simulation of the ballast settlements in void zones. However, because of the computational cost, the track model is usually limited to a small size of ballast box with one sleeper without slopes or a 2D model for many ones. It complicates the investigation that includes the railway track together with many sleepers connected with elastic rail for a void zone. Additionally, both in the simple phenomenological approach and the detailed DEM simulations, it is unclear how the initial compaction after maintenance works in some moments of the track life cycle could be taken into account.

The present study aims an investigation the sleeper permanent settlements' behavior under the loadings in the void zones using the DEM approach. The overall structure of the research and the detailed interrelations are shown in Fig. 3.

The manuscript consists of studies of short-term interactions, long-term ones, and the following interpretation. The detailed research steps are as follows:

**Fig. 3** Flow chart of the research steps



- (i) Ballast loading patterns in a void zone are generated by using a vehicle-track interaction model (VTI) and substantiated by experimental measurements. The loading patterns correspond to the possible cases of void sizes.
- (ii) The loading patterns from the different parts of the void zone along the track are analyzed and parametrized to quantify the main loading factors—cyclic loading, impact loading, unloading mode, and preloading.
- (iii) DEM simulations of the settlement accumulation are performed for the many cycles of the loading patterns, and the statistics of the settlement intensity are collected.
- (iv) Analysis of the influence of the loading parameters on the settlement intensity is performed, and the parametrized equations are derived.

## 2 Short-Time Dynamic Interaction and Loading Patterns in the Different Parts of the Void Zone

### 2.1 Experimental Measurements and Simulation of Dynamic Interaction in the Void Zone

The experimental measurements of the train-track dynamic interaction in void zones, which were presented in the previous studies (Sysyn et al. 2020, 2021a, 2021b), demonstrate the appearance of the specific impact interaction. The influence of unsupported sleepers on the dynamics and stability of railway tracks is indicated in many other studies (Xu et al. 2023; Liu et al. 2023; Malekjafarian et al. 2021; Sresakoolchai and Kaewunruen 2022). The main feature of the dynamic interaction in void zones is different from the simple geometric irregularities in that the impact oscillations appear before the wheel enters the central part of the void zone. Thus, the maximal dynamic interaction appears in the first half of the void zone, while the maximal interaction in the geometrical irregularity is usually located in the second part of the irregularity while the wheel outside is moving. The typical behavior in

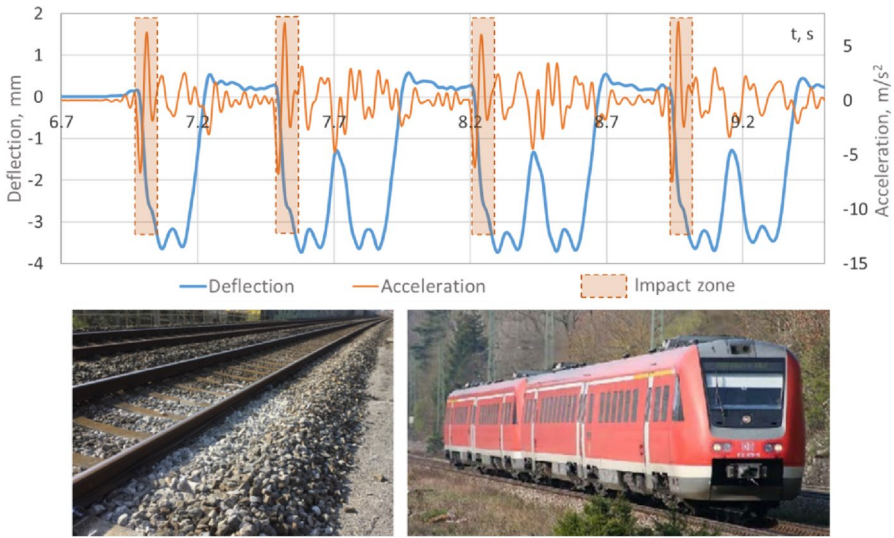
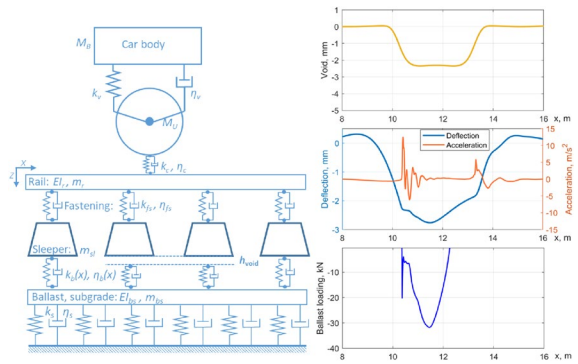


**Fig. 4** Measured rail deflections and accelerations in the void zone (top), the ballast pulverization in the void zone (bottom, left), the corresponding to the measurement rolling stock (bottom, right)

**Fig. 5** Vehicle-track interaction model (VTI) with void under the sleepers (left) and simulation example: right, top—void along the track; right, center—rail deflection/acceleration in section  $x = 11.5$  m; right, bottom—ballast loading in section  $x = 11.5$  m (Sysyn et al. 2021a, 2021b)



the void zone is obviously explained by rail deflection measurements (Fig. 4). The impact interaction (Fig. 4, top) is clearly presented by rail accelerations that precede time to the maximal rail deflections. More detailed analysis of experimental measurements is presented in Sysyn et al. (2020).

The reason for the dynamic behavior is the closing of the voids between the sleeper’s foot and the ballast bed while the wheel enters the void zone. The behavior can be explained by using simple models like those explained in Sysyn et al. (2020); Sysyn et al. 2021b). The present study uses a 3-beam model coupled with two discrete masses that was described in Sysyn et al. 2021a. Figure 5 presents the schematic presentation of the model and a simulation example of rail deflections and ballast loadings for wheel passing the void zone. The void is considered by nonlinear stiffness in the layers corresponding to the model. The simulations clearly show

the dynamic interaction while the wheel enters the void zone and the corresponding sleeper-ballast impact. A full description of the model is presented in Sysyn et al. 2021a; Sysyn et al. 2021b).

## 2.2 Loading Patterns of Ballast Layer in the Void Zone

The aim of the present section is to study the loading patterns of the ballast layer in the void zone, their systematization, and preparation for the following estimation of long-term settlements using DEM simulations. The void zone size and form could be very different during the track lifecycle. The experimental studies (Wang and Markine 2018; Varandas et al. 2014) show that the void length could reach 8 m and depth 10 mm in transition zones. The typical form of the void is unknown. Therefore, the rectangular void form with smoothed ends is used in the VTI simulation. The actual length of the void zone with hanging sleepers under their own weight is varied in the range of 1.2–4.5 m, and the depth is limited to 5 mm according to experimental measurements. From the overall 25 combinations of the length/depth, which was described in Sysyn et al. 2021a, the 109 most different ballast loading patterns were selected for the analysis and further simulations.

The vehicle track interaction model parameters are selected to provide qualitative agreement with the experimental measurements, reference information about the superstructure elements, and parameter estimation from other studies (Sysyn et al. 2021a, 2021b; Lichtberger 2005; Malekjafarian et al. 2021; Zhai 2020; Zakeri et al. 2020). The properties of the model beams and the vehicle masses are considered for one rail and wheel. The superstructure parameters correspond to rail UIC60, half sleepers B70, and fastening pads Zw.700. The loading of the vehicle corresponds to the freight wagon with a train velocity of 120 km/h.

The vehicle parameters were selected according to Sysyn et al. 2021a; Sysyn et al. 2021b; Malekjafarian et al. 2021; Zhai 2020; Zakeri et al. 2020) and are as follows: car body mass for one wheel 10,000 kg; unsprung wheel mass 650 kg; contact stiffness  $50 \times 10^9$  N/m; contact damping  $110 \times 10^3$  N s/m; suspension stiffness  $0.8 \times 10^6$  N/m; and suspension damping  $30 \times 10^3$  N s/m.

The track parameters were chosen according to Lichtberger (2005) and are the following: rail meter mass (layer 1) 60 kg/m; rail bending stiffness (layer 1)  $6.4 \text{ MN}\cdot\text{m}^2$ ; fastening foundation coefficient (layer 1)  $200 \text{ MN}/\text{m}^2$ ; fastenings damping (layer 1)  $185 \text{ kN}\cdot\text{s}/\text{m}^2$ ; sleeper meter mass (layer 2) 300 kg/m; sleeper-ballast foundation coefficient (layer 2)  $600 \text{ MN}/\text{m}^2$ ; sleeper-ballast damping (layer 2)  $75 \text{ kN}\cdot\text{s}/\text{m}^2$ ; ballast meter mass (layer 3) 500 kg/m; ballast-subgrade foundation coefficient (layer 3)  $200 \text{ MN}/\text{m}^2$ ; and ballast-subgrade damping (layer 3)  $680 \text{ kN}\cdot\text{s}/\text{m}^2$ .

The ballast loading patterns could be categorized into three groups that depend on the position along the void zone: preloaded ballast in the neighbor zone (Fig. 6, top), impact zone (Fig. 6, middle), and unloaded zone (Fig. 6, bottom). The ballast preloading in the neighbor-to-void zones varies in a range of up to 20 kN (Fig. 6, top). The preloading. The impact loading is presented by a peak with full unloading before and cyclic loading after. Actually, there are only two groups—with and without the full unloading. The group of the full unloading without impact is selected by



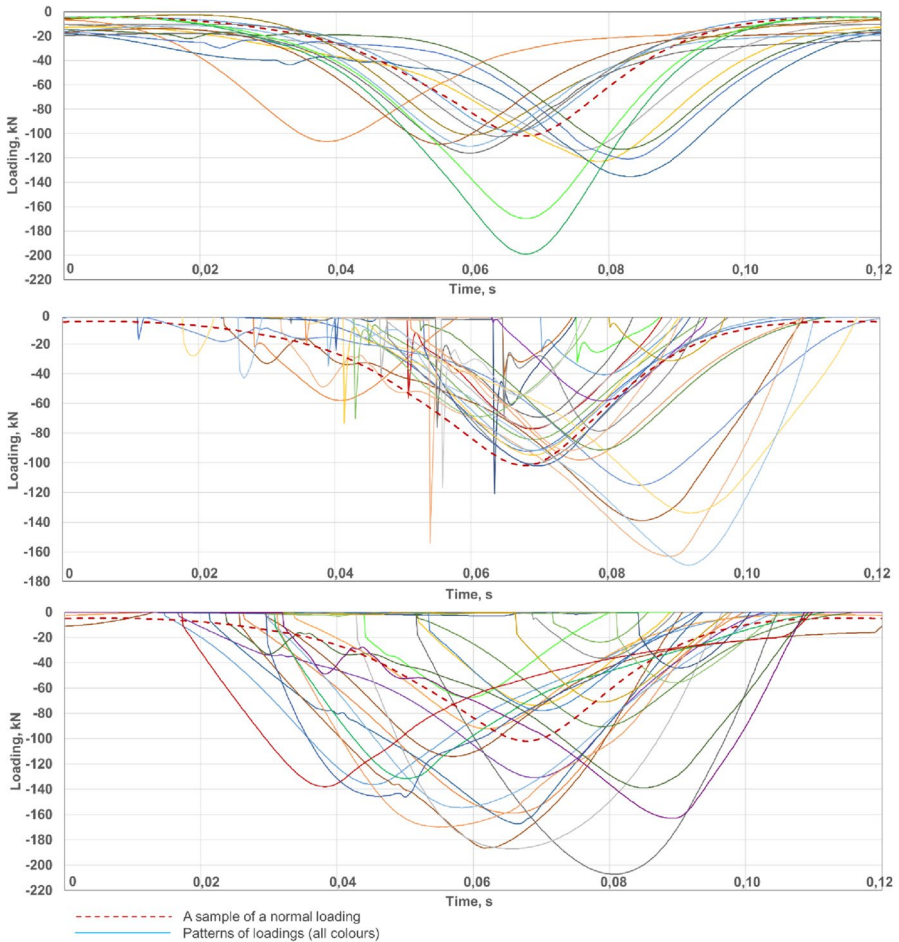


**Fig. 6** Groups of loading patterns along the void zone: preloaded ballast in the neighbor zone (top), impact zone (middle), unloaded zone without impact (bottom)

the evident absence of the peaks. The relative position of the impact peaks and the maxima of the quasistatic loading are different—from superposition with the cyclic loading to separate impact peaks before them.

### 2.3 Parametrization of Loading Patterns

The loading patterns should be described with a limited number of parameters for the following estimation of the quantitative relations between the ballast loading and the settlement intensity. The most evident parameters that describe the loading pattern (see Fig. 6) and differ between the three loading groups are as presented in Fig. 7:

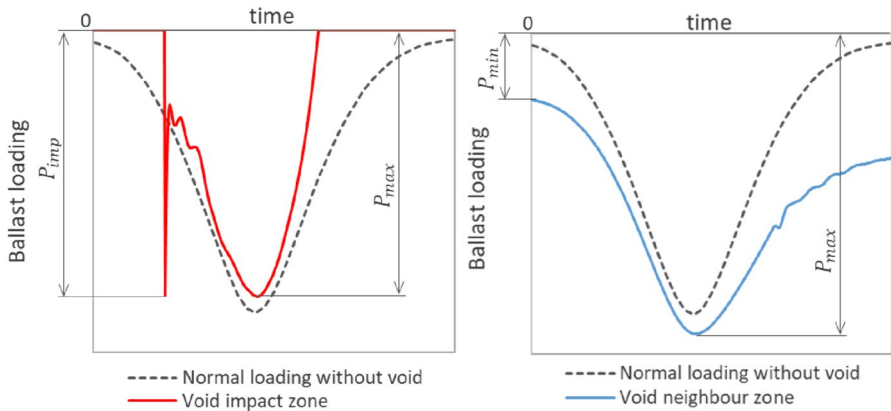


**Fig. 7** Parameters of loading patterns for a void zone (left) and a neighbor zone (right)

- (i) The maximal value of the quasistatic loading  $P_{max}$ .
- (ii) The peak value of the impact loading  $P_{imp}$ .
- (iii) The minimal loading in the absence of the wheel loading  $P_{min}$ .

Thereby, the stepwise increase of the loading ( $> 3.5$  kN) after full unloading is also considered as an impact loading parameter  $P_{imp}$ .

The presented in Fig. 7 parametrization scheme allows simple and evident derivation of the loading parameters. However, the scheme does not allow the separation of the parameters according to the factors of vibration and the cyclic loading since the  $P_{imp}$  includes a part of the superposed cyclic loading. On the other side, considering only the impact amplitude would bring more uncertainties for the cases without evident impact peaks. More objective separation of the impact and the cyclic loading could be possible by spectral methods that, however, could cost the interpretability of the parameters. The additional studied parameter is the sleeper maximal acceleration that was received from the vehicle-track model.

### 3 Long-Term Settlement Accumulation in the Void Zone

#### 3.1 Experimental Exploration of the Void Geometry Development

The practice of the maintenance of the track with void zones shows that the zones are characterized by intensive track quality deterioration. The neighbor is only possible if the depth of the void zone is quicker growing than its length. The present section aims the exploration of the interrelation of the void length to its depth.

The measurements of rail deflections were produced in 12 places of problem zones of rail track. The zones were in different conditions of void severity from void initiation to the time moment before the tamping. Thus, the void zones have different sizes and forms during the lifecycle. It is not possible with the available measurements to urge about the evolution of the void development since the data are the

snapshots in the lifecycle without the known loading history. Nevertheless, the data enable the exploration of the general relations of the void depth and length during the lifecycle and, thus, the conclusion about the void's possible development.

The deflection measurements in 12 void zones are shown on Fig. 8, middle, and the corresponding reference zones are presented on Fig. 8, top. The problem places are presented on continuous ballasted track without or with some initial reasons for the void initiation, like rail welds and subgrade problems. The transition zones are not considered.

The depth of the void zones under the sleeper is determined as the difference between the rail maximal deflections in the void zone and the reference one ( $\Delta h_{\text{void}}$ ). The length of the void zones under the sleeper is the difference of the recorded waves at the level  $-0.1$  mm to reduce the uncertainty of the zero point  $x$ -coordinate estimation due to low inclination noise ( $\Delta l_{\text{void}}$ ). The relation of the void length to its depth is shown in Fig. 9. The considered void depth is up to 5 mm, and the void length is up to 4 m.

Figure 9 indicates that the relation of the void depth to its length is nonlinear. The void depth is quickly increasing for a length of more than 2 m, which indicates the acceleration of the differential settlement intensity in the void zone. The range of the growth of the void length is much lower than the relative variation of the void depth. The results indicate that the settlement intensity of the neighbor-to-void sleepers is much lower than that of the hanging sleepers. The causes of this effect are evidently different settlement intensities in the void zone and outside because of various loading patterns: impact loading, full unloading, and preloading. The quantitative estimation of the settlement intensities depending on the loading parameters is produced with the help of DEM simulations.

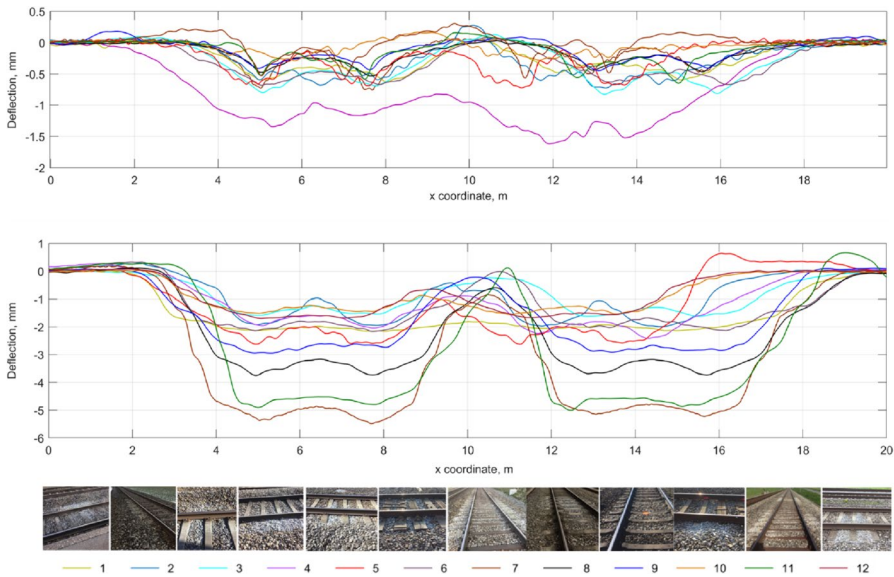
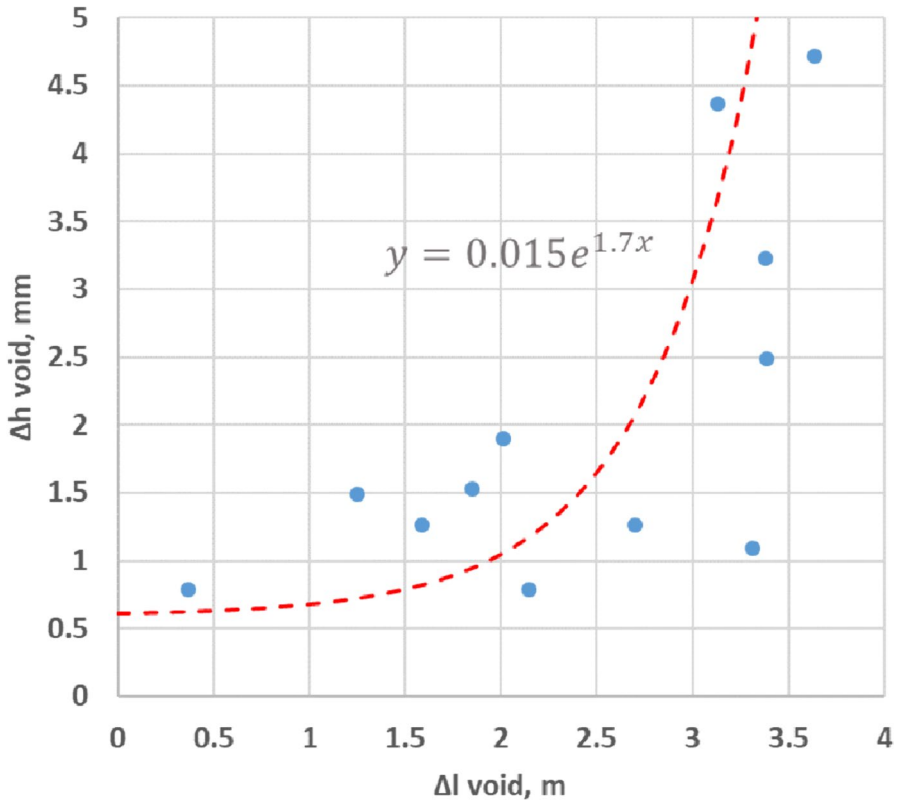


Fig. 8 Rail deflection measurements in 12 void zones and the corresponding reference zones



**Fig. 9** Relation of the void length difference ( $\Delta l_{\text{void}}$ ) to its depth difference ( $\Delta h_{\text{void}}$ ) for the void in different severity

### 3.2 DEM Model and Simulation of Settlement Accumulation

The aim of this section is an estimation of the long-term influences of the ballast loading in the void zone that are described by a settlement intensity of the residual deformations. The intensity is defined as the linear accumulation of the vertical residual deformations per 10,000 loading cycles after the stabilization stage. Thereby, to avoid the problem of the initial compaction uncertainty, stage 1 of the initial settlement accumulation is neglected. The ballast layer in the DEM is maximally compacted before the cyclic loading so that the permanent settlement accumulation could be close to linear in stage 2. The result of a simulation is the settlement intensity. The complexity of the model is selected to be able to reflect the studied effects of void accumulation under the loading patterns. Due to the high computational cost of the DEM model and many loading patterns, it is maximally simplified with round particles and a stiff sleeper. The following assumptions and limitations are noted:

- (i) – To take into account the loading patterns of the ballast that already consider the superstructure weight, the sleeper mass in the DEM model is low.
- (ii) – The sleeper is an undeformable body.
- (iii) – The ball particles are used with rolling resistance to reflect the particles' angularity.
- (iv) – The ballast compaction process is not considered; the ballast bed is introduced in maximally compacted form with a special compaction procedure to provide close to linear accumulation of the settlements in the following loading cycles. Within the procedure, the maximal compaction was achieved by setting the particle and boundary friction close to zero (similar to liquid) and by inserting the sleeper with vibrating motion in the ballast bed with temporary slope boundaries, limiting particles flow.
- (v) – The ballast layer, after compaction, is stabilized with a set of cyclic loadings corresponding to the normal loading case (100 kN/rail) in the vehicle track model.
- (vi) – Particle breakage and attrition are not taken into account.

The DEM model for the simulation of the ballast settlements under the cyclic and dynamic loadings is presented by one sleeper in a ballast box (Fig. 10). The sleeper geometry corresponds to the B70 sleeper. The particle form is simple balls with a standard size distribution of 22.5–63 mm. The ball particles are described by rolling radii, nonlinear contact law, tangential stiffness, rolling resistance, etc. Mindlin–Deresiewicz model is used to describe the tangential force. Hertzian spring with viscous damping was used as the normal force model. The rolling resistance takes into account the influence of the particle form. The parameters of the model parameters are selected according to experimental and theoretical studies (Xiao et al. 2023; Zhang et al. 2023a, 2022; Chi et al. 2022; Chi et al. 2022; Guo et al. 2022; Xiao et al. 2023; Sluganović et al. 2019).

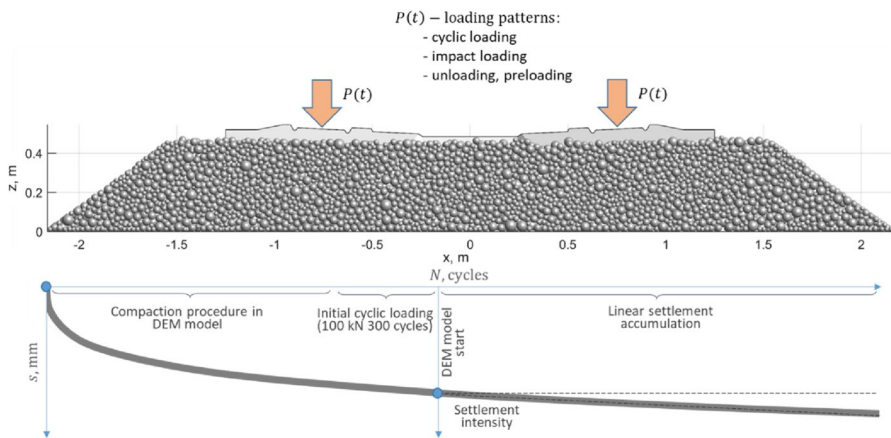


**Fig. 10** DEM model for simulation of the sleeper settlements (top). DEM model preparation for determining the settlement intensity (bottom)

The mechanical properties of the sleepers are the following: density 2650 kg/m<sup>3</sup>, Young's modulus 20 GPa, and Poisson's ratio 0.3. The degrees of freedom of the sleeper motion are limited to the vertical motion and rotation relative to the track axis. The particle properties are the following: the bulk density of 1700 kg/m<sup>3</sup>, Young's modulus of 50 GPa, and Poisson's ratio of 0.3. The particle interaction properties are the following: static friction 0.65, dynamic friction 0.61, rolling resistance 0.41, and restitution coefficient 0.72.

The material properties of boundaries are as follows: right/left trog walls—Young's modulus of 20 GPa, Poisson's ratio of 0.3, bulk density of 1700 kg/m<sup>3</sup>; Young's modulus of trog bottom is 10 GPa and trog bottom bulk density of 1600 kg/m<sup>3</sup>. The interaction parameters between the boundaries and the ballast particles are the following: between trog bottom and particles—static friction 0.6, dynamic friction 0.58, and restitution coefficient 0.72 and between right/left trog walls and particles—friction close to zero, and restitution coefficient 0.65.

The interaction parameters between sleeper and ballast particles are taken as follows: static friction 0.60, dynamic friction 0.58, and restitution coefficient 0.72. The ballast layer is filled in a ballast trog of a width of 60 cm, and the ballast height under the sleeper is about 30 cm.

The sleeper in the DEM simulations is considered a rigid body, and all external loadings are applied to its center. The sleeper is considered to be weightless to transmit the ballast loading patterns (from Sect. 2.2, Fig. 6) without taking into account the sleeper mass twice. In this way, the loading on the sleeper (Fig. 10) is considered to be equal to the loading on the ballast bed. The external loading on the sleeper depicts the vertical loading on rail seats with a loading cycle of 0.1 s.

The sleeper sides are filled with particles to provide a ballast bed with 40-cm ballast shoulders and slopes. Ballast bed with sleeper is maximally compacted before simulations. The number of particles depends on the sleeper type: 21,287 particles for a wide sleeper and 25,788 for a conventional sleeper.

The sleeper deflection simulation results for the typical loading patterns are presented in Fig. 11. The settlement intensity is determined as a trend line over the last part of the cyclic line of the sleeper deflections to exclude the initial nonlinear settlements. Thus, the settlement intensity for the normal cyclic loading (Fig. 11a) and own weight preloading is about 0.17 mm/10,000 cycles. The increase of the cyclic loading to 170 kN (Fig. 11b) causes more intensive permanent settlement accumulation with an intensity of about 2.1 mm/10,000 cycles. The additional low-impact loading together with normal loading (Fig. 11d) causes many times higher settlement accumulation than without the impact. The double increase of the impact loading (Fig. 11e) causes more than three times the increase in the settlement intensity. Thereby, the nonlinear settlement trend appears at the beginning of the deflection line. However, the increase of the additional preloading  $P_{min}$  of the sleeper, which is typical for the neighbor-to-void zones, causes some reduction of the settlement intensity compared to high loading and normal preloading (Fig. 11c).

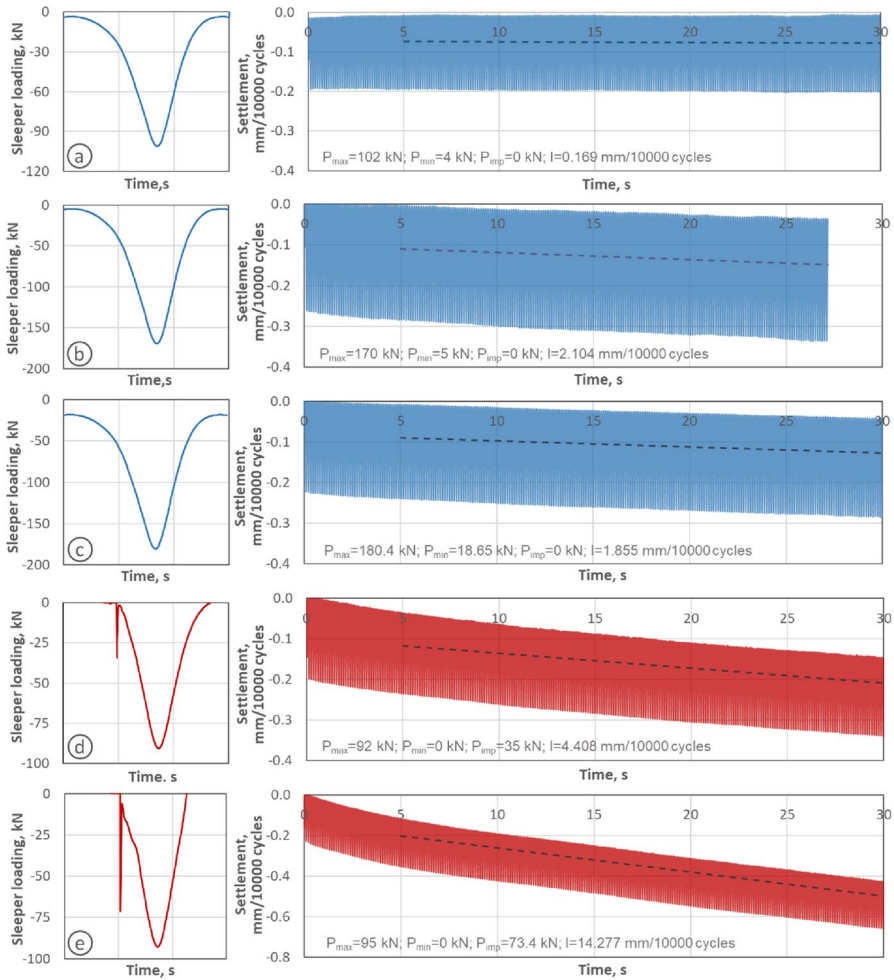


**Fig. 11** Settlement accumulation processes (right) for typical loading patterns (left): **a** normal cyclic loading, **b** high cyclic loading, **c** preloading, **d** low-impact loading, and **e** high-impact loading

## 4 Analysis of the Settlement Intensity

### 4.1 Explorative Analysis of Influence of the Loading Parameters on the Settlement Intensity

The formed in DEM and MBS simulation dataset, before fitting by statistical models, is qualitatively analyzed on the interrelations between factors. Figure 12 presents a multiplot of the pairwise interrelation of the settlement intensity and the loading parameters. The histograms in the main diagonal show the statistical distribution of the corresponding factor. Thus, the intensity histogram shows that most cases of the settlement processes have settlement intensities less than 4 mm/10,000 cycles.

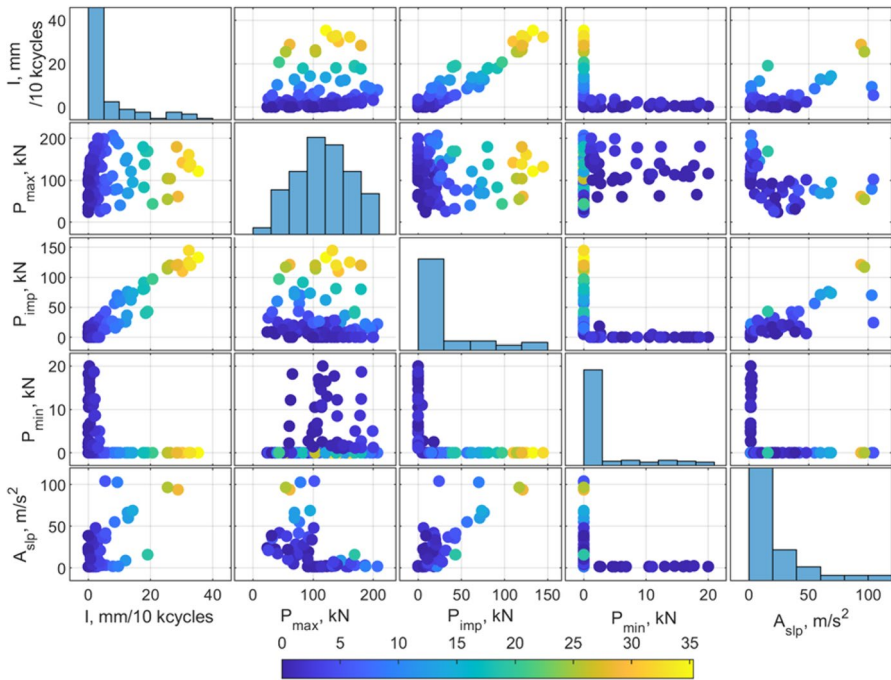


**Fig. 12** Interrelation of the settlement intensity and the loading parameters

The parameter of cyclic loading  $P_{\max}$  is in the range of 40–200 kN/sleeper, with an average value of about 100 kN. The impact loading  $P_{\text{imp}}$  is in the range of 0–150 kN, and the minimal constant preloading  $P_{\min}$  0–20 kN. Thereby, both factors exclude one another—the impact is possible if minimal preloading is absent. The increase of minimal preloading  $P_{\min}$  slightly decreases the settlement intensity, especially for low values of  $P_{\min}$ . Thereby, unloading  $P_{\min}$  well contributes to reduction of the settlement intensity for high  $P_{\max}$  (Fig. 12, row 2, column 2).

The impact loading parameter  $P_{\text{imp}}$  has the highest influence on settlement intensity (Fig. 12, row 1, column 3). The influence of the cyclic loading  $P_{\max}$  is several times lower than that of  $P_{\text{imp}}$ . The sleeper acceleration parameter  $A_{\text{slp}}$  indicates an insignificant influence in the intensity in a range up to 35  $\text{m/s}^2$ . Moreover, high acceleration does not always result in high settlement intensities and impact loadings (Fig. 12, row 1, column 3).

The parameters  $P_{\text{imp}}$  and  $P_{\max}$  are independent ones, as is shown from the point cloud (Fig. 12, row 3, column 2). The parameters  $P_{\text{imp}}$  and  $A_{\text{slp}}$  (Fig. 12, row 1, column 3) present evident correlation and could be considered as dependent parameters. However, for impact loading less than 35 kN, the relationship between the parameters is weak. Noticeable is the relationship between  $P_{\max}$  and  $A_{\text{slp}}$  (Fig. 12, row 1, column 2): high sleeper accelerations appear for thy cyclic loadings less than 120 kN.

Principal component analysis (PCA) is performed to explore the common variation of the parameters without taking into account the settlement intensities. PCA



is one of the most widely used unsupervised learning methods. Figure 13 shows the diagrams of the data points in the pairwise spaces of the principal components as well as the all three ones. The colormap of the intensities highlights each data point. The direction and weight of each variable (parameter) are presented with vectors. The most significant weight in the data variation has the variables  $P_{\max}$  and  $P_{\text{imp}}$ . The corresponding vectors show, in three directions, the most significant response variation (settlement intensity). The sleeper acceleration variable  $A_{\text{slp}}$  has a different direction than other variables and can be considered as an independent one. The minimal preloading variable  $P_{\min}$  has a comparatively low weight.

## 4.2 Machine Learning Approach Based on the Parameters' Dataset

The qualitative analysis of the datasets from DEM and MBS simulations shows the evident influence of the cyclic, impact loading, vibration, and preloading mode on the settlement intensity. Various methods can be used to explore the qualitative relations between the parameters and the settlement intensity. Machine learning tools are usually used for the solution of many problems in railway engineering (Tang et al. 2022; Phusakulkajorn et al. 2023). The application of statistical and machine learning methods for studying the behaviors of ballast layers with or without unsupported sleepers and zones with stiffness transitions is presented in Sresakoolchai and Kaewunruen (2022); Soufiane et al. 2023; Zhang et al. 2023b; Palese 2023; Miao et al. 2023; Sresakoolchai et al. 2023; Milosevic et al. 2023; Lesiak et al. 2023). Track geometry deterioration is studied in Zhao et al. (2023); Jover and Fischer 2022) using data-driven methods and statistical analysis. Application of advanced deep learning methods for track element diagnostics, monitoring, and prediction of the residual life cycle is demonstrated in the studies (Tabaszewski and Firlik 2022; Zhang et al. 2021; Wang et al. 2023; Rahman et al. 2023; Zare Hosseinzadeh et al. 2023; Silva-Rodríguez et al. 2023; Awd et al. 2022).

**Fig. 13** Principal component analysis of the settlement intensity and the loading parameters

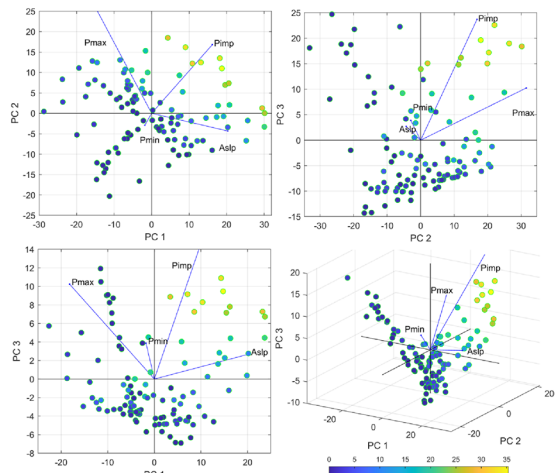


**Table 2** Benchmark of machine learning models for the dataset  $P_{\max}-P_{\min}-A_{\text{slp}}$ 

No	Model type/fivefold cross-validation	RMSE	MSE	$R^2$	MAE
1	Gaussian process regression (GPR): exponential	3.89	15.17	0.57	2.44
2	Neural network: narrow	3.96	15.73	0.55	2.11
3	Linear regression	4.18	17.48	0.50	2.44
4	SVM: quadratic	4.39	19.32	0.45	2.52

**Table 3** Benchmark of machine learning models for the dataset  $P_{\max}-P_{\min}-P_{\text{imp}}$ 

No	Model type/fivefold cross-validation	RMSE	MSE	$R^2$	MAE
1	Gaussian process regression (GPR): exponential	1.51	2.22	0.97	0.99
2	Neural network: narrow	1.81	3.29	0.96	1.20
3	Linear regression	2.14	4.58	0.95	1.52
4	SVM: quadratic	2.15	4.61	0.94	1.28

The Regression Learner App from the Statistics and Machine Learning Toolbox of Matlab is used to automatically train various regression models to make predictions of the settlement intensities using supervised machine learning. The tool allows the application of many popular machine learning approaches like conventional linear regression, support vector machine (SVM), Gaussian process regression (GPR), and neural networks.

The impact or vibration factor is considered by two alternative parameters and corresponding datasets: with impact loading parameter  $P_{\text{imp}}$  and with sleeper acceleration  $A_{\text{slp}}$ . The models were trained and validated using fivefold cross-validation. Table 2 presents the most successful results of model training and validation for the dataset  $P_{\max}-P_{\min}-A_{\text{slp}}$  by the benchmark of the following metrics: root mean squared error (RMSE), mean squared error (MSE), coefficient of determination  $R^2$ , and mean absolute error (MAE). However, the  $R^2$  coefficient presents rather moderate prediction quality for the dataset  $P_{\max}-P_{\min}-A_{\text{slp}}$  with the GPR model.

Table 3 presents the best results of the model validation for the dataset  $P_{\max}-P_{\min}-P_{\text{imp}}$ . The prediction quality, different from the alternative dataset (see Table 2) with the sleeper acceleration, is much better. The best results are presented by GPR and the neural network models with RMSE 1.51 and 1.81, which corresponds to the relative error of 4.3% and 5.2% to the overall variation range of the settlement intensity

The best prediction of the settlement intensity for the dataset  $P_{\max}-P_{\min}-P_{\text{imp}}$  using (GPR) is analyzed in detail. The 2D diagrams of the settlement intensities from each factor are presented in Fig. 14. The diagrams show the influence of the pairs of factors with different line colors. The third factor is assumed to be constant:  $P_{\min} = 0$  kN for the diagrams  $I(P_{\max})$  and  $I(P_{\text{imp}})$  (Fig. 14, left, center) and  $P_{\text{imp}} = 0$  kN  $I(P_{\min})$  (Fig. 14, right). Thus, the impact case assumes preloading to be absent and vice versa. Additionally, the diagrams present the initial points of the dataset, predicted ones, and the errors between them. The left and central diagrams show that

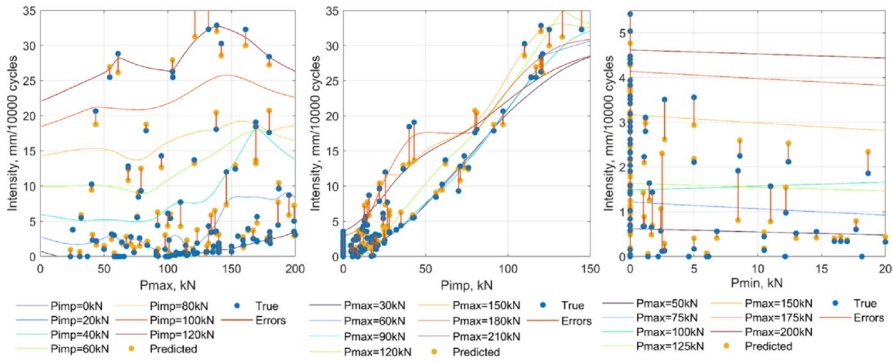


**Fig. 14** Prediction of the settlement intensity using machine learning approach (GPR) for  $P_{min} = 0$  kN (left);  $P_{min} = 0$  kN (center);  $P_{imp} = 0$  kN (right)

the maximal error of the intensity prediction is about 5 mm/10,000 cycles or about 14% for 2–3 points from the all dataset. The maximal error of the intensity prediction depending on the  $P_{min}$  (Fig. 14, right) is about 2.3 mm/10,000 cycles, which is more than 50% compared to the possible variation range of the case with preloading and absent impact.

The diagram lines  $I(P_{imp})$  show an increase in the settlement intensity together with the increase of the impact loading, and the increase in cyclic loading, in general, produces an additional contribution to the increase of the intensity. However, not all trends of the lines are plausibly growing. Moreover, the lines depicting the influence of the cyclic loading  $P_{max}$  (Fig. 14, center) are not monotonic. The diagram  $I(P_{min})$  (Fig. 14, right) demonstrates some decrease in the settlement intensity with the increase of the preloading, but the trend is not consistent for all cases of cyclic loadings.

Thus, the automatized application of the machine learning tools demonstrated good prediction quality. However, the results are only partially mechanically plausible. It is expected that the increase in the impact and cyclic loading should cause a definite increase in the intensity. Therefore, the model is overfitted. More statistical data would probably improve the prediction.

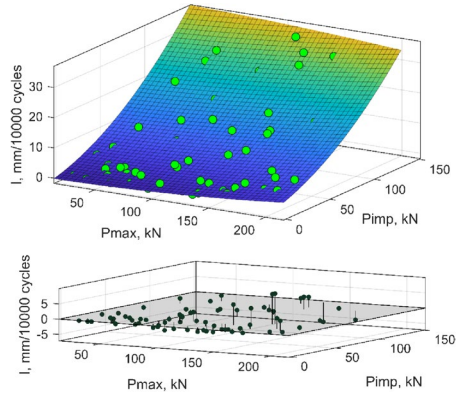
### 4.3 Analytic Approach Based on the Parameters’ Dataset

The presented in the previous section machine learning approach demonstrates accurate but not mechanically plausible prediction results. Moreover, the data-driven model is a black box that does not explain the relationship between the loading factors and the settlement intensity. Therefore, a simple analytic approach is used as a possible alternative to the machine learning one. Simple polynomial and exponential analytical equations fit the dataset of the settlement intensities and the loading parameters. It allows us to search for the best fit within the plausible monotonic trends. Additionally, the dataset is split into two independent datasets with less

**Table 4** Coefficients and fitting quality metrics for Eq. (2)

Equation coefficients		Fitting quality metrics	
$p_{01}$	0.08707	MSE	10.25
$p_{02}$	0.001046	$R^2$	0.98
$p_{11}$	0.0001382	RMSE	1.26
$p_{20}$	$5.447e-07$	Fivefold cross-validation RMSE	2.05

**Fig. 15** Polynomial fitting of the settlement intensity (top) and the residuals (bottom) in relation to maximal cyclic loading  $P_{max}$  and impact loading  $P_{imp}$



number of parameters: the impact case and the preloading case. The expected resulting function of the intensity is supposed to be described by the condition:

$$I(P_{max}, P_{imp}, P_{min}) = \begin{cases} I(P_{max}, P_{imp}), & P_{min} = 0 \\ I(P_{max}, P_{min}), & P_{min} > 0 \end{cases} \quad (1)$$

A polynomial equation fits the dataset with the loading parameters  $P_{max}$  and  $P_{imp}$  that consist of 67 data points. The best fit after excluding the nonmeaningful terms is presented by Eq. (2):

$$I(P_{max}, P_{imp}) = p_{20}P_{max}^3 + p_{01}P_{imp} + p_{11}P_{max}P_{imp} + p_{02}P_{imp}^2 \quad (2)$$

Here,  $P_{max}$ : the maximal value of the quasistatic loading (kN).

$P_{imp}$ : the peak value of the impact loading (kN).

The coefficients of Eq. (2) and the fitting quality metrics are presented in Table 4.

The 3D plot of the fitting surface and the fitting error is shown in Fig. 15. The surface demonstrates the plausible monotonic trends of the settlement intensities in both directions. The influence of the impact loading is much higher than that of the cyclic loading. Thereby, the influence of the cyclic loading is noticeably amplified with high-impact loading. The residuals plot (Fig. 15, bottom) shows the deviation of the points of the dataset from the fitting surface. The highest absolute error is about 6–9 mm/10,000 cycles or about 17–25% relative error for 4 points of the dataset.

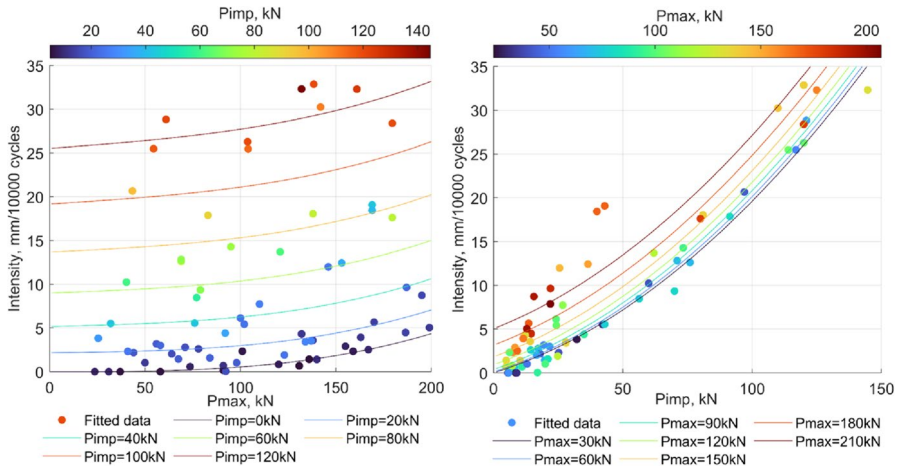


**Fig. 16** Polynomial fitting of the settlement intensity in relation to maximal cyclic loading and impact loading:  $I(P_{max})$ —left and  $I(P_{imp})$ —right

**Table 5** Coefficients and fitting quality metrics for Eq. (3)

Equation coefficients		Fitting quality metrics	
$p_1$	0.02022	MSE	1.97
$p_2$	$2.61e-09$	$R^2$	0.91
		RMSE	0.32
		Fivefold cross-validation RMSE	0.48

The quality of the settlement intensity prediction is better visible in 2D diagrams (Fig. 16), showing the separate influence of each factor. The influence of the levels of the additional factor is shown by different line colors as well as the data points with the corresponding colormap. The diagram (Fig. 16, left) presents the significant increase in the settlement intensity if even low-impact loading is present. The variation of the settlement intensity within the range of the cyclic loadings increased for high-impact loading. The right diagram of the settlement intensity, depending on the impact loading, demonstrates, in general, the plausible trend. However, the presence of a visually separate cluster of data points is noticeable for the impacts less than 50 kN. Most of the outliers belong to the cluster.

The dataset with the loading parameters  $P_{max}$  and  $P_{min}$  involves 37 data points fitted by polynomial and exponential Eq. (3):

$$I(P_{max}, P_{min}) = p_1 P_{max}^4 \cdot e^{-p_2 P_{min}} \tag{3}$$

Here,  $P_{min}$  is the minimal loading in the absence of the wheel loading (kN).

The coefficients of Eq. (3) and the fitting quality metrics are presented in Table 5.

**Fig. 17** Polynomial fitting of the settlement intensity (top) and the residuals (bottom) in relation to maximal cyclic loading  $P_{\max}$  and preloading  $P_{\min}$

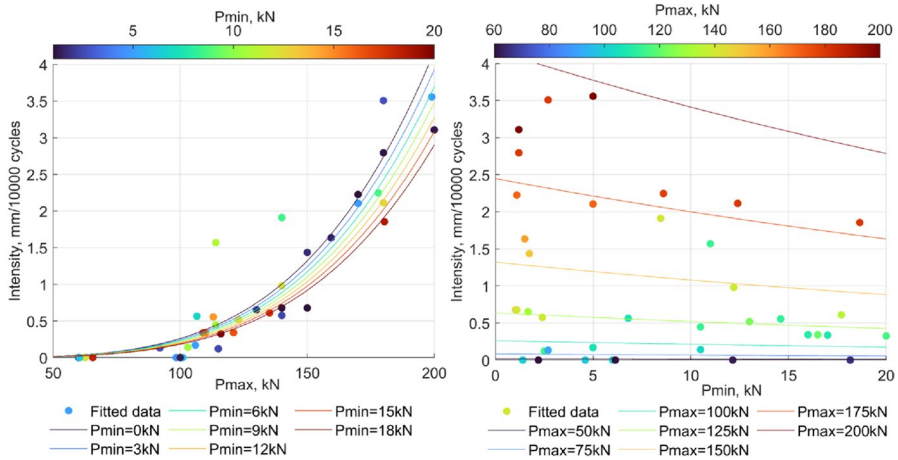
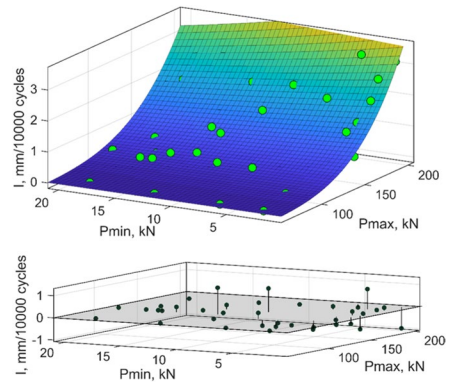


**Fig. 18** Polynomial fitting of the settlement intensity in relation to maximal cyclic loading and minimal loading:  $I(P_{\max})$ —left and  $I(P_{\min})$ —right

Equation (3) is presented in the form of a diagram in Fig. 17, together with the data points and the diagram of residuals. The diagram shows the monotonic non-linear increase of settlement intensity together with the cyclic load and gradual decrease related to the minimal loading. The influence of the cyclic loading dominates. However, the influence of minimal preloading is noticeable in the cases of high cyclic loadings. The residual plot (Fig. 17, bottom) shows the deviation of the points of the dataset from the fitting surface. The highest absolute error is about 0.9–1.2 mm/10,000 cycles or about 23–30% relative error for 5 points of the dataset.

The diagram (Fig. 18, left) presents the clear power increase of the settlement intensity according to the data points. The reduction of the minimal preloading amplifies the influence of the maximal cyclic loading. The diagram of the settlement intensity depending on the minimal preloading (Fig. 18, right) shows the

plausible trend of the settlement intensity reduction altogether, although the cloud of the data points is widely scattered and could imply different possible trends.

A comparison of the predicted settlement intensities for the case with 100 kN of the cyclic loading on the sleeper and the absent impact loading shows the values  $< 0.1\text{--}0.2$  mm/10,000 cycles that correspond to the upper values of the range (0.002–0.162 mm/10,000 cycles) of the values from Table 1. The result could be explained that the settlement accumulation during applied 300 cycles in case of low cyclic loadings  $< 70$  kN was so insignificant and ambiguous that it was considered zero. Additionally, it should be noted that the particle/sleeper/subgrade material properties (friction, rolling resistance) were relatively low in the possible range presented in the literature (up to 0.8 static friction). It is expected that the reliable estimation of the settlement intensities in the range 0.002–0.01 mm/10,000 cycles would require 3000–30,000 cycles in the DEM model.

## 5 Discussion and Results

Analysis of the previous studies shows that the ballast bed in zones with unsupported sleepers experience complex loadings consisting of cyclic, dynamic ones, and full and partial unloading. The sensitivity of the bearing capacity of the structural elements from the cohesionless soils and ballast materials to impact and vibration loadings is well known from many geotechnical studies.

Nevertheless, the loading of the ballast bed in zones with voids is considered the same as the simple geometric irregularities while predicting the settlement accumulation and track geometry deterioration. Despite many proposed phenomenological equations, not all explicitly consider loading, and those considering it present the influence of the ballast loading with the power functions with the wide exponent variance from 0.3 to 5.12. Moreover, the direct settlement influence of the vibration, impact, and sleeper unloading, which appear in the void zones, was almost not considered in the settlement equations. The impact loadings are usually handled the same as cyclic loading.

The present studies demonstrate a high variance of predicted and measured processed settlement accumulations. Thereby, the highest variance appears in the initial stage of ballast settlement accumulation ( $< 100,000$  loading cycles). Moreover, even then same measurement repetitions show a high variance of the initial settlements and a relatively low variance of the further settlement accumulation.

The novelty of the present study:

- (i) The ballast bed loading patterns of the short-time dynamic interaction in the void zone were classified and parametrized: impact, full unloading, and preloading.
- (ii) An approach for estimation of the long-term ballast settlement processes by using DEM simulations is proposed and used for determining the settlement intensities for the loading patterns.
- (iii) Estimation of settlement intensity in relation to impact, cyclic loading, and preloading is presented by machine learning and analytic approaches.

## 5.1 Analysis of the Experimental Information

The present study is based on the experimental studies of rail deflection measurements in void zones (Sysyn et al. 2020, 2021a, 2021b). The experimental studies show that the short-time dynamic interaction in void zones is characterized by impacts and vibrations together with cyclic loading (Fig. 4).

Thereby, the maximal impact and cyclic loading appear at different times: the impact loading precedes the cyclic one. The sleeper-ballast impact loading appears due to void closing. Dynamic loading, because of geometric irregularity, different from void interaction, appears during wheel rolling-out of the irregularity.

Experimental studies do not present the long-term measurements of the processes in void zones. However, the multiple measurements of rail deflections in zones with voids with different severities of the whole life cycle (Fig. 8) can provide an indirect indication of the long-term processes of void evolution. Figure 9 indicates that the void depth is accelerating compared to its length during the life cycle from low severity to high severity. It is only possible if the settlement in the neighboring void zones (with preloading) is less intensive than in void zones with impact and full unloading.

The previous experimental studies of other authors did not differentiate between the wheel-rail dynamic interaction and the sleeper-ballast one that appears in different time moments and locations along the void zone.

## 5.2 Short-Time Dynamic Interaction and Loading Patterns

The VTI simulations of the short-time interaction in the void zones of the different sizes provided different loading processes of the ballast layer. A simple 1-wheel model with the separated masses of ballast and sleeper was used to preserve the clear interpretability of the loading patterns and the limited number of loading parameters. The experimental measurements show that the highest sleeper-ballast impact appears before the first axle of the bogie, and further impact can appear only after full-track unloading. Thus, different combinations of the axle distances would need additional loading parameters, which could be the aim of many further studies.

The loading patterns could be visually categorized into three groups that depend on the sleepers' position along the void zone: preloaded ballast in the neighbor zone (Fig. 6, top), impact zone (Fig. 6, middle), and unloaded zone (Fig. 6, bottom). The loading patterns could be split into two groups—with the full unloading and without. The impact group pattern is very different—the relative position of the impact peaks is usually in superposition within the wave of the quasistatic loading. While some patterns present rather isolated impacts and quasistatic processes.

A simple intuitive parametrization of the loading patterns was applied (Fig. 7)—the value of the loading peaks for impact loading  $P_{imp}$  and the quasistatic loading  $P_{max}$ , as well as the minimal pre-loading  $P_{min}$ . As an alternative parameter corresponding to the impact interaction  $P_{imp}$ , the maximal sleeper acceleration  $A_{slp}$ .

The previous studies of other authors considered dynamic interaction and vibration in void zones as a result of wheel-rail interaction but not sleeper-ballast



interaction. Thus, void irregularity was considered like a geometric irregularity. Our present and previous studies clearly show that sleeper-ballast impacts appear in time before the maximal cyclic loading and the following wheel-rail dynamic interaction. However our previous studies on void zones (Sysyn et al. 2020, 2021a, 2021b) did not systemize all cases of interaction in void zone. The present study classified the loading patterns into three groups and proposed parametrization of loading patterns.

### 5.3 Long-Term Processes of Settlement Accumulation

The present study takes into account the problem of uncertainty in the initial stage (which was described in the introduction) and, therefore, intentionally discards it from consideration. The settlement accumulation intensity is considered in the close-to-linear second stage. A 3D DEM model of one sleeper in a ballast box with slopes is used to estimate the intensity. The ballast layer in the model is prepared maximally compacted and stabilized with initial cyclic loading. It results in the close to linear settlement accumulation within the low number of cycles. Due to the high computational cost of the DEM model and many loading patterns, it is maximally simplified with round particles and a stiff sleeper. The model is applied for the settlement simulation of more than 100 loading patterns.

The simple but computationally quick DEM model with round particles was used to estimate the settlement intensity for many variants of the ballast loading processes. The model does not take into account many factors like particle breakage and attrition and real form. Still, it can consider the effect that was aimed in the study—ballast flow-induced settlements of sleeper, impact, and vibration influence. The results (Fig. 11) show a clear increase in the settlement intensity by the application of even low-impact loading. At the same time, the ballast preloading causes a positive effect on the settlement intensity reduction, especially for high cyclic loadings. The effect agrees well with the results of the experimental measurements indicating low settlement intensity in neighbor sleepers to void zones. However, it should be noted that the settlement accumulation during the applied 300 cycles in the case of low cyclic loadings  $< 70$  kN was so insignificant and ambiguous that it was considered zero.

The simulation results indirectly correspond to the experimental measurements. The available experimental measurements of track deflection in void zones of various severities present indicators about the possible trends of the void size evolution. The results (Fig. 9) indicate that the settlement intensity of the neighbor-to-void sleepers should be much lower than that of the hanging sleepers. Thus, the void zone should grow in depth quicker than in width, which agrees with the simulation results.

The data interpretation and recovery of the relations between the settlement intensity and the loading parameters are produced with the machine learning approach and the analytic one. The explorative analysis clearly shows that the used four loading parameters are independent factors. It was supposed that the impact/vibration factor could be described either with the first impact  $P_{\text{imp}}$  or, alternatively, sleeper acceleration  $A_{\text{slp}}$ . However, the machine learning approaches

(Table 4) show moderate prediction quality of the dataset with the parameter of sleeper acceleration  $A_{slp}$ . At the same time, the dataset with the parameter  $P_{imp}$  presents good cross-validation prediction accuracy with  $R^2=0.97$  and  $RMSE=1.51$  for the exponential GPR model. Moreover, the error of the prediction of the single data points is not more than 14%. However, the detailed analysis of the relations between the predicted intensity and parameters (Fig. 14) shows that relations are not monotonous and mechanically not fully plausible.

However, the data-driven approach can better describe the local details like the data cluster cluster of the outliers for  $P_{imp} < 50$  kN for the analytical model (Fig. 16, right). Larger datasets would improve the quality of the machine-learning approach.

The applied analytic approach with simple polynomial and exponential relations allows to control the plausible relations and the function monotonicity. The splitting of the datasets into two separate groups and the fitting with different functions allows the increase of the prediction quality. The validation RMSE of the prediction quality for the analytic approach is about 25% lower than for the machine learning approach, but its mechanical plausibility is better. Moreover, the analytic functions with the 4 and 2 number coefficients (Eqs. (1) and (2)) allow a clear interpretation of the relations.

The diagram (Fig. 16, right) shows a cluster of the outliers for  $P_{imp} < 50$  kN that does not fully correspond to the general trend. It could be explained by the result of a very simple parametrization of the impact part  $P_{imp}$  (Fig. 7). The parametrization scheme (Fig. 7) considers only one impact peak that is partially overlapped with the wave of the cyclic loading. However, the impact loading process (Fig. 6, center) is much more complex than the assumed pattern: relative position, form, and number of impacts can be different. The application of more advanced parametrization with more parameters could improve the prediction accuracy. However, more parameters would require longer datasets.

The additional drawback of the presented parametrization scheme is that the presented Eq. (2) does not allow to factorize it in form  $I = f(P_{max})f(P_{imp})$  with two independent factors as proposed in Holtendorff (2003). It is expected that the impact/vibration without cyclic loading cannot cause settlements. However, the diagrams (Fig. 16) show high settlement intensities even if  $P_{max} = 0$ . It could be explained with the used parametrization (Fig. 7), in which the impact parameter  $P_{imp}$  contains some part of the superposed cyclic loading. Other parametrization schemes would probably resolve the drawback.

Summarizing all above, it has to be pointed out that the cyclic loading has a non-linear influence on the settlement intensity that corresponds to the 3–4 power function of the ballast loading and corresponds to many studies (Table 1). The impact loading has the influence close linear or parabolic trend. The minimal unloading has an evident influence on the reduction of the settlement intensity for the cases of high cyclic loadings that could be described by inverse exponential relation. The estimated settlement accumulation for the reference case agrees in general with the literature values. However, it should be noted that the absolute accuracy of the approach is limited to the intensity value of about 0.1 mm/10,000 cycles. Thus, the conclusions of the present study are valid for the cyclic loadings not less than 100–120 kN.

## 6 Conclusions

An approach for estimation of the ballast settlement intensity in void zones is presented in the paper. Different from the previous studies with phenomenological equations that take into account only the maximal loading, the approach takes into account the cyclic ballast loading, impact loading, and minimal preloading in form of simple analytic relations.

The following major conclusions are drawn from the present study:

- (1) Present phenomenological equations do not take into account ballast impacts, vibration, and unloading. The influence of the cyclic loading factor is estimated by power functions of very different degrees, from 0.3 (decelerating trend) to 5.12 (accelerating trend).
- (2) The experimental measurements of rail deflections indicate that the settlement intensity of the neighbor-to-void sleepers is much lower than that of the hanging sleepers.
- (3) DEM simulation model was used to estimate the ballast settlement intensity after settlement stabilization for more than 100 loading processes of the void zone. The DEM simulations show a clear influence of the impact loading on the settlement intensity.
- (4) The cyclic loading has a nonlinear influence on the settlement intensity that corresponds to the 3–4 power function, and the impact loading is expressed by the parabolic function.
- (5) Ballast minimal preloading contributes to the reduction of the settlement intensity, especially for high cyclic loadings that are typical for neighbor-to-void zones.
- (6) The analytic approach and splitting the data separate datasets with and without preloading allow to receive plausible simple analytic equations of the settlement intensity with good prediction accuracy.

**Acknowledgements** The authors would like to acknowledge the support from the Philipp Schwartz Initiative of the Alexander von Humboldt Foundation.

**Funding** Open Access funding enabled and organized by Projekt DEAL.

### Declarations

**Conflict of Interest** The authors declare no competing interests.

**Open Access** This article is licensed under a Creative Commons Attribution 4.0 International License, which permits use, sharing, adaptation, distribution and reproduction in any medium or format, as long as you give appropriate credit to the original author(s) and the source, provide a link to the Creative Commons licence, and indicate if changes were made. The images or other third party material in this article are included in the article's Creative Commons licence, unless indicated otherwise in a credit line to the material. If material is not included in the article's Creative Commons licence and your intended use is not permitted by statutory regulation or exceeds the permitted use, you will need to obtain permission directly from the copyright holder. To view a copy of this licence, visit <http://creativecommons.org/licenses/by/4.0/>.

## References

- Alzabeebee, S.: Calibration of a finite element model to predict the dynamic response of a railway track bed subjected to low-and high-speed moving train loads. *Transp. Infrastruct. Geotechnol.* **10**(3), 504–520 (2023)
- Awd, M., Münstermann, S., Walther, F.: Effect of microstructural heterogeneity on fatigue strength predicted by reinforcement machine learning. *Fatigue Fract. Eng. Mater. Struct.* **45**(11), 3267–3287 (2022)
- Baeßler, M., Rücker, W.: Track settlement due to cyclic loading with low minimum pressure and vibrations. In "System dynamics and long-term behaviour of railway vehicles, track and subgrade" (Hrsg: Popp, K., Schielen, W.), Heidelberg, Springer-Verlag, 2002
- Bian, X., et al.: Analysing the effect of principal stress rotation on railway track settlement by discrete element method. *Géotechnique* **70**(9), 803–821 (2020). <https://doi.org/10.1680/jgeot.18.P.368>
- Chen, C., Indraratna, B., McDowell, G., Rujikiatkamjorn, C.: Discrete element modelling of lateral displacement of a granular assembly under cyclic loading. *Comput. Geotech.* **69**, 474–484 (2015)
- Chen, C., McDowell, G.R.: An investigation of the dynamic behaviour of track transition zones using discrete element modelling. *Proc. Inst. Mech. Eng. Part F J. Rail Rapid Transit.* **230**, 117–128 (2016)
- Chi, Y., Xiao, H., Zhang, Z., Fang, S., Wang, H.: Discrete element analysis on mechanical properties of ballast bed by tamping in railway turnout areas. *J. Comput. Nonlinear Dyn.* **17**(11), 111005 (2022)
- Y Chi, H Xiao, Z Zhang, S Fang, H Wang. Discrete element analysis on mechanical properties of ballast bed by tamping in railway turnout areas. *J. Comput. Nonlinear Dyn.* 2022
- Dahlberg, T.: Some railroad settlement models—a critical review. *Proc. Inst. Mech. Eng. Pt. F:J Rail Rapid Transit.* **215**(4), 289–300 (2001)
- de Oliveira Barbosa, J.M., Fărăgău, A.B., van Dalen, K.N., Steenberg, M.J.M.M.: Modelling ballast via a non-linear lattice to assess its compaction behaviour at railway transition zones. *J. Sound Vib.* **530**, 116942 (2022). <https://doi.org/10.1016/j.jsv.2022.116942>
- Demharter, K.: Setzungsverhalten des Gleisrostes unter vertikaler Lasteinwirkung. Technischen Universität München, Prüfamt für Bau von Landverkehrswegen (1982)
- Fang, J., Zhao, C., Lu, X., Xiong, W., Shi, C.: Dynamic behavior of railway vehicle-ballasted track system with unsupported sleepers based on the hybrid DEM-MBD method. *Constr. Build. Mater.* **394**, 132091 (2023). <https://doi.org/10.1016/j.conbuildmat.2023.132091>
- Fang, Jun, Zhao, Chunfa, Shi, Can, Zhai, Zhihao, Cai, Changsheng: Dynamic impact of sleeper unsupported defects on the heavy haul locomotive-ballasted track coupling system. *Soil Dyn. Earthq. Eng.* **176**, 108292 (2024)
- Frohling, R.D. Deterioration of railway track due to dynamic vehicle loading and spacially varying track stiffness. PhD Thesis in the Faculty of Engineering University of Pretoria, Pretoria, 1997.
- Grossoni, I., Andrade, A.R.: Bezin Y and Neves S The role of track stiffness and its spatial variability on long-term track quality deterioration. *Proc. IMechE Pt. f: J Rail Rapid Transit* **233**(1), 16–32 (2019)
- Grossoni, I., Powrie, W., Zervos, A., Bezin, Y., Le Pen, L.: Modelling railway ballasted track settlement in vehicle-track interaction analysis. *Transp. Geotech.* **26**, 100433 (2021). <https://doi.org/10.1016/j.trgeo.2020.100433>
- Guerin, N., Sab, K., Moucheron, P.: Experimental identification of a settlement law for ballast (frz.). *Can. Geotech. J.* **36**, 3 (1999)
- Guo, Y., Shi, C., Zhao, C., Markine, V., Jing, G.: Numerical analysis of train-track-subgrade dynamic performance with crumb rubber in ballast layer. *Constr. Build. Mater.* **336**, 127559 (2022)
- Hadi, M.A., Alzabeebee, S.: Development of a finite element model to study the settlement of ballasted railway tracks subjected to two adjacent moving trains. *Transp. Infrastruct. Geotechnol.* **10**(5), 733–748 (2023)
- Hettler, A.: Schottertriaxialversuche mit statischem und zyklischem Belastungsverlauf. *Eisenbahntechnische Rundschau*, 1987, Heft 36, 399–405.
- Indraratna, B., Nimbalkar, S.: Stress-strain degradation response of railway ballast stabilized with geosynthetics. *J. Geotech. Geoenviron. Eng.* **139**(5), 684–700 (2013)
- Indraratna, B., Shahin, M.A., Salim, W.: Stabilisation of granular media and formation soil using geosynthetics with special reference to railway engineering. *J. Ground Improv.* **11**(1), 27–44 (2007)
- Jeffs T and Marich S. Ballast characteristics in the laboratory. In: Conference on railway engineering 1987: preprints of papers. Australia: Institution of Engineers 1987

- Jover, V., Fischer, S.: Statistical analysis of track geometry parameters on tramway line No 1 in Budapest. *Balt J. Road Bridge Eng.* **17**(2), 75–106 (2022)
- Kangle Chen Evaluation of the short-term and long-term behaviour of vehicle-track-system at track transitions based on numerical simulations. PhD Thesis. Technischen Universität München. 2022
- Khan, M.R., Dasaka, S.M.: High-speed train vibrations in the sub-soils supporting ballasted rail corridors. *Transp. Infrastruct. Geotechnol.* **10**(2), 259–282 (2023)
- Kira Holtzendorff. Untersuchung des Setzungsverhaltens von Bahnschotter und der Hohllagenentwicklung auf Schotterfahrbahnen. Dissertation. Technische Universität Berlin. – Berlin, 2003 D 83. – 130 s.
- Kumar, N., Kossmann, C., Scheriau, S., Six, K.: An efficient physical-based method for predicting the long-term evolution of vertical railway track geometries. *Proc. Inst. Mech. Eng. Pt. f: J. Rail Rapid Transit* **236**(4), 095440972110248 (2021). <https://doi.org/10.1177/09544097211024803>
- Kurhan, D., Kurhan, M., Husak, M.: Impact of the variable stiffness section on the conditions of track and rolling stock interaction. *IOP. Conf. Ser. Mater. Sci. Eng.* **985**(1), 012005 (2020). <https://doi.org/10.1088/1757-899X/985/1/012005>
- Lesiak, P., Bojarczak, P., Sokolowski, A.: Algorithm for the extraction of selected rail track ballast degradation using machine vision. *Transp. Problems* **18**(1), 129–141 (2023)
- Lichtberger, B.: *Track Compendium: Formation, Permanent Way, Maintenance, Economics*. Eurailpress, Hamburg, Germany (2005)
- Liu, J., Du, S., Liu, G., Wei, X., Liu, H.: Influence of unsupported sleepers on the dynamic stability of ballasted bed based on wheelset impact tests. *Railway Eng. Sci.* **31**(1), 52–6 (2023)
- Lobo-Guerrero, S., Vallejo, L.E.: Discrete element method analysis of railtrack ballast degradation during cyclic loading. *Granul. Matter* **8**, 195–204 (2006). <https://doi.org/10.1007/s10035-006-0006-2>
- Lundqvist, A., Dahlberg, T.: Load impact on railway track due to unsupported sleepers. *Proc. Inst. Mech. Eng. Pt. F J. Rail Rapid Transit* **219**(2), 67–77 (2005). <https://doi.org/10.1243/095440905x8790>
- Malekfarhan, A., OBrien, E.J., Quirke, P., Cantero, D., Golpayegani, F.: Railway track loss-of-stiffness detection using bogie filtered displacement data measured on a passing train. *Infrastructures* **6**, 93 (2021). <https://doi.org/10.3390/infrastructures6060093>
- Miao, S., Gao, L., Tong, F., Ma, C., Chen, Z.: Ballastless track mortar layer void detection by high-order statistical analysis of axle box acceleration. *Measurement* **211**, 112681 (2023)
- Milosevic, M., Pålsson, B., Nissen, A., Johansson, H., Nielsen, J.C.O. Model-based remote health monitoring of ballast conditions in railway crossing panels. *Lecture Notes in Civil Engineering*. 253 LNCE, pp. 502–512.2023.
- Moghadam, M.J., Ashtari, K.: Numerical analysis of railways on soft soil under various train speeds. *Transp. Infrastruct. Geotechnol.* **7**(1), 103–125 (2020)
- Nasrollahi, K., Nielsen, J.C.O., Aggestam, E., Dijkstra, J., Ekh, M.: Prediction of long-term differential track settlement in a transition zone using an iterative approach. *Eng. Struct.* **283**, 115830 (2023). <https://doi.org/10.1016/j.engstruct.2023.115830>
- Nguyen, K., Villalmanzo, D.I., Goicolea, J.M., Gabaldon, F.: A computational procedure for prediction of ballasted track profile degradation under railway traffic loading. *Proc. IMechE Pt. f: J. Rail Rapid Transit* **230**(8), 1812–1827 (2016)
- Ognibene, G., Le Pen, L., Harkness, J., Zervos, A., Powrie, W.: An Alternative Approach to Track Settlement Prediction. *Lect. Notes Civ. Eng.* **165**, 99–112 (2022). [https://doi.org/10.1007/978-3-030-77234-5\\_9](https://doi.org/10.1007/978-3-030-77234-5_9)
- ORE: Optimale Anpassung des klassischen Oberbaus an den künftigen Verkehr. Frage D117, Report Nr. 5 und 10.
- Pahnke U. Frequenzspektren des Schotteroberbaus / Ulf Pahnke, Frank Müller-Boruttau Norbert Breitsamer // Eisenbahntechnische Rundschau, 2010. – №7–8. – S. 473–483.
- Palese, J.W.: A method for using transformed track deflection data to assess dynamic forces at railway track stiffness transitions. *Transp. Infrastruct. Geotech.* **11**(1), 110–31 (2023). <https://doi.org/10.1007/s40515-023-00274-6>
- Phusakulkajorn, W., Núñez, A., Wang, H., Jamshidi, A., Zoeteman, A., Ripke, B., Dollevoet, R., De Schutter, B., Li, Z.: Artificial intelligence in railway infrastructure: current research, challenges, and future opportunities. *Intell. Transp. Infrastruct.* **2**, liad016 (2023)
- Popp K. System dynamics and long-term behavior of railway vehicles, track and subgrade (Lecture Notes in Applied Mechanics; vol. 6). / K. Popp, W. Schiehlen. — Berlin Heidelberg: Springer-Verlag, 2003. — 488 p.

- Punetha, P., Nimbalkar, S.: An innovative rheological approach for predicting the behaviour of critical zones in a railway track. *Acta Geotech.* (2023). <https://doi.org/10.1007/s11440-023-01888-3>
- Rahman, M.M., Amjadian, M., Pokhrel, M., Tarawneh, C.: Machine learning technique for damage detection of rails on steel railroad bridges subjected to moving train load. *Proc. SPIE Int. Soc. Opt. Eng.* **12487**, 124870R (2023)
- Sato, Y. Japanese studies on deterioration of ballasted track. *Vehicle System Dynamics*, 1995. 24 Suppl. (1): p. 197–208.
- Sayeed, M.A., Shahin, M.A.: Dynamic response analysis of ballasted railway track-ground system under train moving loads using 3D finite element numerical modelling. *Transp. Infrastruct. Geotechnol.* **10**(4), 639–659 (2023)
- Selig, E.T., Waters, J.M.: *Track geotechnology and substructure manage-* Literaturverzeichnis 129 ment. Tomas Telford, London (1994)
- Shahin, M.A.: Design of ballasted railway track foundations under cyclic loading. In: 2009 GeoHunan International Conference - Slope Stability, Retaining Walls, and Foundations, pp. 68–73. American Society of Civil Engineers, Changsha, Hunan, China (2009). [https://doi.org/10.1061/41049\(356\)11](https://doi.org/10.1061/41049(356)11)
- Shenton, M.: *Ballast Deformation and Track Deterioration*, in *Track Technology*. Thomas Telford Ltd, London (1984)
- Silva-Rodríguez, J., Salvador, P., Naranjo, V., Insa, R.: Supervised contrastive learning-guided prototypes on axle-box accelerations for railway crossing inspections. *Exp. Syst. Appl.* **207**, 117946 (2023)
- Sluganović, V., Lakušić, S., Lazarević, D.: Track ballast modelling by discrete element method. *Gradjevinar* **71**(7), 589–600 (2019). <https://doi.org/10.14256/JCE.2350.2018>
- Soufiane, K., Zarembski, A.M., Palese, J.W. Forecasting cross-tie condition based on the dynamic adjacent support using a theory-guided neural network model 2023. *Proc. Inst. Mech. Eng. Pt. F: J. Rail Rapid Transit*
- Sresakoolchai, J., Kaewunruen, S.: Prognostics of unsupported railway sleepers and their severity diagnostics using machine learning. *Sci. Rep.* **12**(1), 6064 (2022)
- Sresakoolchai, J., Hamarat, M., Kaewunruen, S.: Automated machine learning recognition to diagnose flood resilience of railway switches and crossings. *Sci. Rep.* **13**(1), 210 (2023)
- Stewart, H. and E. Selig, *Correlation of Concrete Tie Track Performance in Revenue Service and at the Facility for Accelerated Service Testing - Volume II: Prediction and Evaluation of Track Settlement*. 1984, US Department of Transportation Federal Railroad Administration: Washington, DC.
- Sysyn, M., Gerber, U., Kovalchuk, V., Nabochenko, O.: The complex phenomenological model for prediction of inhomogeneous deformations of railway ballast layer after tamping works. *Arch. Transp.* **46**(3), 91–107 (2018)
- Sysyn, M., Gerber, U., Gruen, D., Nabochenko, O., Kovalchuk, V.: Modelling and vehicle based measurements of ballast settlements under the common crossing. *European Transport - Trasporti Europei* (71), (2019)
- Sysyn, M., Nabochenko, O., Kovalchuk, V.: Experimental investigation of the dynamic behaviour of railway track with sleeper voids. *Railway Eng. Sci.* **28**(3), 290–304 (2020). <https://doi.org/10.1007/s40534-020-00217-8>
- Sysyn, M., Przybyłowicz, M., Nabochenko, O., Liu, J.: Mechanism of sleeper–ballast dynamic impact and residual settlements accumulation in zones with unsupported sleepers. *Sustain.* **13**, 7740 (2021a). <https://doi.org/10.3390/su13147740>
- Sysyn, M., Przybyłowicz, M., Nabochenko, O., Kou, L.: Identification of sleeper support conditions using mechanical model supported data-driven approach. *Sensors* **21**(11), 3609 (2021b). <https://doi.org/10.3390/s21113609>
- Tabaszewski, M., Firlik, B.: Detection of the presence of rail corrugation using convolutional neural network. *Eng. Trans.* **70**(4), 339–353 (2022)
- Tang, R., De Donato, L., Bešinović, N., Vittorini, V., Wang, Z.: A literature review of artificial intelligence applications in railway systems. *Transp. Res. Part C Emerg. Technol.* **140**, 103679 (2022)
- Talebahhoie, E., Thiery, F., Meng, J., Nordlund, E., Rantatalo, M.: Modelling of railway sleeper settlement under cyclic loading using a hysteretic ballast contact model. *Sustain.* **13**(21), 12247 (2021)
- Thom, N. and J. Oakley. Predicting differential settlement in a railway trackbed, in *Railway foundations conference: Railfound*. 2006.
- Tutumluer, E., Qian, Y., Hashash, Y.M., Ghaboussi, J., Davis, D.D.: Discrete element modelling of ballasted track deformation behaviour. *Int. J. Rail Transp.* **1**(1–2), 57–73 (2013). <https://doi.org/10.1080/23248378.2013.788361>

- Varandas, J.N., Hölscher, P., Silva, M.A.: Settlement of ballasted track under traffic loading: application to transition zones. *Proc. Inst. Mech. Eng. Pt. f J. Rail Rapid Transit.* **228**(3), 242–259 (2014). <https://doi.org/10.1177/0954409712471610>
- Wang, H., Markine, V.: Modelling of the long-term behaviour of transition zones: prediction of track settlement. *Eng. Struct.* **156**, 294–304 (2018)
- Wang, H., Li, B., Gong, J., Xuan, F.-Z.: Machine learning-based fatigue life prediction of metal materials: perspectives of physics-informed and data-driven hybrid methods. *Eng. Fract. Mech.* **284**, 109242 (2023)
- Xiao, J., Xue, L., Zhang, D., Bai, Y., Shi, J.: Coupled DEM-FEM methods for analyzing contact stress between railway ballast and subgrade considering real particle shape characteristic. *Comput. Geotech.* **155**, 105192 (2023)
- Xiao, H., Zhang, Z., Zhu, Y., Gan, T., Wang, H.: Experimental analysis of ballast bed state in newly constructed railways after tamping and stabilizing operation. *Constr. Build. Mater.* **362**, 129772 (2023)
- Xu, C., Ito, K., Hayano, K., Momoya, Y.: Combined effect of supported and unsupported sleepers on lateral ballast resistance in ballasted railway track. *Transp. Geotech.* **38**, 100913 (2023)
- Zakeri, J.A., Fattahi, M., Nouri, M., Janatabadi, F.: Influence of rail pad stiffness, axle loads on dynamic responses of train-track interaction with unsupported sleepers. *Period. Polytech. Civil Eng.* **64**(2), 524–534 (2020). <https://doi.org/10.3311/PPci.14826>
- Zare Hosseinzadeh, A., Datta, D., Lanza di Scalea, F.: In-motion railroad tie deflection measurement via ultrasonic airborne sonar and computer vision techniques. *Res. Nondestruct. Eval.* **34**(1), 1–21 (2023)
- Zhai, W., 2020. Practical Applications of the Theory of Vehicle–Track Coupled Dynamics in Engineering. In: *Vehicle–Track Coupled Dynamics*. Springer, Singapore. [https://doi.org/10.1007/978-981-32-9283-3\\_10](https://doi.org/10.1007/978-981-32-9283-3_10)
- Zhang, X., Zhao, C., Zhai, W.: Importance of load frequency in applying cyclic loads to investigate ballast deformation under high-speed train loads. *Soil Dyn. Earthq. Eng.* **120**, 28–38 (2019)
- Zhang, D., Di, C., Hamadache, M., Stewart, E. Degradation assessment of train axle bearing based on a deep transfer learning. *proceedings of the 31st European Safety and Reliability Conference, ESREL 2021*, pp. 3179–3184, 2021.
- Zhang, Z., Xiao, H., Zhu, Y., Nadakatti, M.M.: Hufe Macro–meso mechanical properties of ballast bed during three-sleeper tamping operation. *Int. J. Rail Transp.* **11**(6), 886–91 (2022)
- Zhang, Z., Xiao, H., Wang, Y., Nadakatti, M.M., Jin, J.: Numerical simulation of the three-sleeper asynchronous tamping operation of ballast bed based on the virtual unit module and polyhedral ballast model. *Transp. Geotech.* **40**, 100964 (2023a)
- Zhang, D., Xu, P., Tian, Y., Zhong, C., Zhang, X.: Ballasted track behaviour induced by absent sleeper support and its detection based on a convolutional neural network using track data. *Urban Rail Transit* **9**(2), 92–109 (2023b)
- Zhao, W., Qiang, W., Yang, F., Jing, G., Guo, Y. Data-driven ballast layer degradation identification and maintenance decision based on track geometry irregularities. *Int. J. Rail Transp.* 2023
- Zhu, J.Y., Thompson, D.J., Jones, C.J.: On the effect of unsupported sleepers on the dynamic behaviour of a railway track. *Veh. Syst. Dyn.* **49**, 1389–1408 (2011). <https://doi.org/10.1080/00423114.2010.524303>

## Authors and Affiliations

Olga Nabochenko<sup>1</sup> · Mykola Sysyn<sup>1</sup>  · Szabolcs Fischer<sup>2</sup>

✉ Mykola Sysyn  
mykola.sysyn@tu-dresden.de

Olga Nabochenko  
olga.nabochenko@mailbox.tu-dresden.de

Szabolcs Fischer  
fischersz@sze.hu

<sup>1</sup> Institute of Railway Systems and Public Transport, Technical University of Dresden,  
Hettnerstraße 2, 01069 Dresden, Germany

<sup>2</sup> Department of Transport Infrastructure and Water Resources Engineering, Faculty  
of Architecture, Civil and Transport Engineering, Szechenyi Istvan University, Egyetem Ter 1,  
Gyor 9026, Hungary